AGU100 ADVANCING EARTH AND SPACE SCIENCE

JGR

Journal of Geophysical Research: Atmospheres

RESEARCH ARTICLE

10.1002/2017JD027501

Key Points:
- Urbanization increases T_2 and PBLH but decreases RH_2 and WS_{10}, which further increases O_3 and decreases $PM_{2.5}$ in urban Beijing
- Compared with normal (clean) days, UHI intensity is enhanced by 11.1% during heat waves in summer (16.7% during polluted days in winter)
- Increasing urban albedo decreases UHI intensity but worsens the urban air quality

Supporting Information:
- Supporting Information S1

Correspondence to:
M. Zhang,
mgzhang@mail.iap.ac.cn

Citation:
Chen, L., Zhang, M., Zhu, J., Wang, Y., & Skorokhod, A. (2018). Modeling impacts of urbanization and urban heat island mitigation on boundary layer meteorology and air quality in Beijing under different weather conditions. *Journal of Geophysical Research: Atmospheres*, *123*, 4323–4344. https://doi.org/10.1002/2017JD027501

Received 24 JUL 2017
Accepted 3 MAR 2018
Accepted article online 25 MAR 2018
Published online 19 APR 2018

Modeling Impacts of Urbanization and Urban Heat Island Mitigation on Boundary Layer Meteorology and Air Quality in Beijing Under Different Weather Conditions

Lei Chen[1,2], Meigen Zhang[1,2,3], Jia Zhu[4], Yongwei Wang[5,6], and Andrei Skorokhod[7]

[1]State Key Laboratory of Atmospheric Boundary Layer Physics and Atmospheric Chemistry, Institute of Atmospheric Physics, Chinese Academy of Sciences, Beijing, China, [2]University of Chinese Academy of Sciences, Beijing, China, [3]Center for Excellence in Urban Atmospheric Environment, Institute of Urban Environment, Chinese Academy of Sciences, Xiamen, China, [4]Research Institute of Climatic and Environmental Governance, Nanjing University of Information Science and Technology, Nanjing, China, [5]Yale-NUIST Center on Atmospheric Environment, Nanjing University of Information Science and Technology, Nanjing, China, [6]School of Atmospheric Physics, Nanjing University of Information Science and Technology, Nanjing, China, [7]Laboratory of Atmospheric Gas Species, A.M. Obukhov Institute of Atmospheric Physics, Russian Academy of Sciences, Moscow, Russia

Abstract Beijing has experienced a rapid urbanization in the last few decades and has been suffering from serious air pollution during recent years. The Weather Research and Forecasting-Chem model is used to quantify the effects of urbanization on regional climate and air quality and those of urban heat island (UHI) mitigation strategy on urban air quality in Beijing, with a special focus on the impacts under different weather conditions (heat waves in summer and polluted days in winter). The modification of rural land use into urban impervious surface significantly increases 2-m temperature (T_2) and planetary boundary layer height but decreases 2-m relative humidity (RH_2) and 10-m wind speed (WS_{10}) in urban Beijing, which further leads to the increases in surface-layer O_3 concentrations of 9.5 ppbv in summer and 1.8 ppbv in winter and the decreases in $PM_{2.5}$ concentrations of 16.6 $\mu g\ m^{-3}$ in summer and 26.2 $\mu g\ m^{-3}$ in winter. Compared with normal days (clean days), the UHI intensity is enhanced by 11.1% during heat waves in summer (by 16.7% during polluted days in winter). Although increasing urban albedo is an effective mitigation strategy to decrease UHI intensity, it worsens the urban air quality. When the urban albedo increases from 0.2 to 0.85, the daily average $PM_{2.5}$ concentrations are increased by 10.2 (6.1) $\mu g\ m^{-3}$ in summer (in winter), and the daily maximum O_3 concentrations are increased by 12.8 ppbv under heat waves in summer.

1. Introduction

Urbanization refers to the population shift from rural to urban areas, which makes towns and cities larger. This process has been recognized as an extreme example of land use and land cover change caused by human activities (Li & Bou-Zeid, 2013; Sharma & Joshi, 2016). In China, the urban population is almost tripled from 1985 to 2015, with the built-up areas expanding from 9386 to 52,102 km^2 (National Bureau of Statistics of China, 2016). By transforming natural vegetation to artificial constructions, urban sprawl dramatically alters the land surface properties, such as heat storage, surface albedo, and roughness length and therefore significantly influences the surface energy budget (Jacobson et al., 2015; Wang et al., 2012), atmospheric circulation (Li et al., 2016), and precipitation (Holst et al., 2016; Miao et al., 2011), which further affects the air quality in urban boundary layer (Liao et al., 2015; Ryu et al., 2013; Zhu et al., 2015).

The most well-known urban climate feature caused by urbanization is the so-called "urban heat island" (UHI), which means the urban area is obviously warmer than its surrounding rural areas (Lin et al., 2016; Oke, 1973; Rotach et al., 2005; Zhang et al., 2015). To quantify the urban-rural differences in temperature (and also other meteorological parameters), one classical method is comparing the observations from urban and rural sites (Chrysanthou et al., 2014; Gaffin et al., 2008; Lin & Yu, 2005; Yan et al., 2009). However, inconsistency in observational records induced by site relocations or instrumental updates may lead to large uncertainties (Ren et al., 2008; Trewin, 2010; Yang et al., 2011). Moreover, it is difficult to designate sites as truly rural stations (Jones et al., 2008; Ren et al., 2007). Because of up-to-date inversion methods and wall-to-wall

coverage of satellite products, remote-sensing techniques are widely used to examine the influence of urbanization. For instance, UHI based on land surface temperature (LST) measurements can be obtained from remote sensors (Lazzarini et al., 2013; Owen et al., 1998; Shen et al., 2016; Zhou et al., 2014). However, coarse temporal resolutions, classification uncertainties in underlying surface types, and impacts of clouds and aerosols during rainy seasons or over heavy polluted regions may generate large biases (Chen, Zhang, Zhu, et al., 2017; Reynolds et al., 2017; Xie et al., 2008).

With the development of high-performance computing technology, conducting numerical simulations by using advanced chemistry-climate models coupled with urban-land modules has been an applicable approach to estimate the impacts of urbanization (Chen et al., 2011). By using the Weather Research and Forecasting (WRF) model, Zhang et al. (2010) investigated the impacts of urbanization on regional climate over YRD (the Yangtze River Delta, China) and found that the mean near-surface temperature in urbanized areas was increased, while the diurnal temperature range was decreased both in summer and winter. Wang et al. (2014) also used the WRF model to estimate the impacts of urban expansion on regional climate over PRD (the Pearl River Delta Region, China). They reported that the reductions in vegetated and irrigated cropland due to urban sprawl significantly reduced near-surface water vapor by 1.5 g kg^{-1} in summer and 0.4 g kg^{-1} in winter. Lin et al. (2008) used the WRF model to analyze the effects of UHI on land sea circulation over northern Taiwan and reported that UHI enhanced the sea breeze in the daytime and weakened the land breeze during the nighttime. WRF simulations were also conducted by Yang et al. (2014) to examine the impact of urbanization on rainfall over the Milwaukee-Lake Michigan region. The thermodynamic perturbations produced by urbanization on surface temperature and pressure could enhance the intrusion of the lake breeze and facilitate the formation of a convergence zone, which were favorable for deep convection in urban areas.

Most previous numerical studies paid attention to the influence of urbanization on urban meteorological fields (Flanner, 2009; Miao et al., 2009; Wang et al., 2012; Yang et al., 2016), while few focused on the effects of urbanization-induced changes in meteorology on air quality. Wang et al. (2007) used mesoscale atmospheric MM5 and chemistry STEM-2K1 models to explore the impacts of urbanization on O_3 concentrations over PRD. The results showed that surface O_3 concentrations were enhanced in the urban expansion regions by 10 ppbv in the daytime and 15 ppbv in the nighttime owing to increased temperature and decreased wind speed. By using a high-resolution chemical transport model (CMAQ), Ryu et al. (2013) showed that enhanced turbulence caused by urbanization diluted NO_x over South Korea, which contributed to the elevated O_3 levels through the reduced O_3 destruction by NO in the NO_x-rich environment. Liao et al. (2015) conducted 2-month simulations using WRF-Chemistry (WRF-Chem) modeling system and reported that urbanization reduced near-surface PM_{10} concentrations over YRD owing to increased PBLH, with a maximum decrease of 57.6 μg m^{-3} during nighttime in July.

These existing modeling studies on urbanization effects over China were mainly focused on the YRD region (Liao et al., 2015; Tao et al., 2015) and the PRD region (Li et al., 2016; Wang, Wu, et al., 2009), and few analyzed the impacts over the North China Plain, especially in Beijing metropolitan area. As the capital of China, Beijing has experienced a continued and rapid urbanization process in the last few decades (Chen, Zhang, Pengwang, et al., 2017; Song et al., 2014) and has been suffering from serious air pollution during recent years (Gao et al., 2015, 2016; Han et al., 2014). It is necessary to examine the influence of urbanization on meteorology and air quality over Beijing.

Previous observational studies indicate that the frequency of heat waves (HWs) has increased during the last few decades (Coumou et al., 2013; Hansen et al., 2010; Yan et al., 2009). IPCC AR5 (the Fifth Assessment Report of the Intergovernmental Panel on Climate Change) suggests that HWs will become more frequent and last longer in the late 21st century. By comparing the observations from an urban site and a rural site, Li et al. (2015) reported that HWs could not only increase the ambient temperature in urban and rural regions but also enhance the UHI intensity (quantified by the difference in urban-rural temperature), implying the synergies between HWs and UHI. In recent years, China has been experiencing severe haze pollution, with fine particulate matter reaching unprecedentedly high levels across many cities, and the frequency of haze events has been reported to increase over the past decades (Cai et al., 2017; Ding & Liu, 2014; Wang et al., 2015). Cao et al. (2016) reported that the haze pollution could enhance UHI in China, implying the synergies between haze pollution and UHI. It is of great interest to quantify the synergistic effects of urbanization and

different weather conditions (i.e., HWs in summer and polluted days in winter) on boundary layer meteorology and air quality in Beijing.

Because of the growing concerns on UHI from scientists and the general public, mitigation strategies to reduce UHI intensity have been proposed, such as urban greening (Fallmann et al., 2016; Sharma et al., 2016) and increasing surface albedo (Taha, 2008; Touchaei et al., 2016). Mackey et al. (2012) pointed out that the cool roof strategy was a viable and cost-effective approach to mitigate the city-scale UHI effect. However, few studies focus on the effects of UHI mitigation measures on urban air quality, and in fact it is an issue that needs attention for urban planner and policy makers.

We present here a study to quantify the effects of urbanization on regional climate and air quality and the influence of UHI mitigation measures on urban air quality in Beijing, with special attention on the impacts under different weather conditions (i.e., HWs in summer and polluted days in winter), using the WRF-Chem model version 3.7 coupling with a single-layer urban canopy model (SLUCM). The descriptions of study area and observation data are presented in section 2. Model configuration is presented in section 3. Section 4 evaluates the model performance and shows the results. The conclusion and discussion are presented in sections 5 and 6, respectively.

2. Description of Study Area and Observation Data

2.1. Description of Study Area

Beijing, as the capital of China, is located in north China and regarded as the political, economic, and cultural center of China. It is also one of the world's most populous capital cities. According to the reports from the official Chinese Government Statistics agency, the population of Beijing at the end of 2015 is approximately 21.7 million, with a sustained and rapid growth of around 20% decade^{-1} since 1960s; its population density of 150 persons/hectare in built-up areas (within the fourth ring road) ranks fourth over China. The urban built-up area of Beijing in 2015 is 1,401 km^2, with an average annual growth rate of 11.6% since 2000. Although the urbanized area in Beijing only accounts for about 2.7% of the total urban area in China, the land use and land cover changes from natural vegetation to impervious surface have a great impact on local climate and air quality over Beijing.

Beijing has a typical temperate and continental monsoon climate, with four distinct seasons and an annual mean temperature of 11.8 °C. Generally, the weather in Beijing is hot and humid in summer, and cold and dry in winter. Beijing has been suffering from serious air pollution during recent years. The annual concentration of $PM_{2.5}$ in Beijing is 80.4 μg m^{-3} in 2015, with 26 days of heavy pollution (defined as a day with 24-hr average $PM_{2.5}$ concentration $>$ 150 μg m^{-3}). The $PM_{2.5}$ pollution in Beijing is especially severe during winter.

2.2. Description of Observation Data

The simulated meteorological parameters, including temperature, relative humidity, wind speed, and wind direction, are compared with daily ground-level meteorological observations at the Beijing Capital International Airport (ZBAA; 39.93°N, 116.28°E), and these data can be collected from the Weather Underground Website (http://www.wunderground.com). Sounding data of temperature, relative humidity, and wind speed at the ZBAA station (station number is 54511) are obtained from the University of Wyoming (http://weather.uwyo.edu/upperair/sounding.html). This meteorological observation site is marked in red triangle in Figure S1a in the supporting information. The hourly measurements of surface-layer O_3 and $PM_{2.5}$ concentrations at 12 sites (1001A–1012A, marked in blue dots in Figure S1b) in Beijing are provided by the China National Environmental Monitoring Center (http://113.108.142.147:20035/emcpublish/). The Aerosol Robotic Network (AERONET), a ground-based remote-sensing aerosol network consisting of worldwide automatic Sun- and sky-scanning spectral radiometers (Holben et al., 1998) provides the aerosol optical depth (AOD) products at 440 and 675 nm, which are used to calculate the AOD at 550 nm with the Angstr□m exponent. The AERONET Level 2.0 AOD data (cloud-screened and quality-assured data) at two sites (Beijing [39.98°N, 116.38°E] and Beijing_CAMS [39.93°N, 116.32°E], marked in black triangles in Figure S1d) are utilized in this study. Hourly downward solar radiation at the Xianghe station ([39.75°N, 116.96°E], marked in purple star in Figure S1c) is taken from World Radiation Monitoring Center-Baseline Surface Radiation Network (http://bsrn.awi.de) and is used to evaluate energy budget simulated by the WRF-Chem model. More details can be found in Tables 1 and S1 in the supporting information.

Table 1
Information for the Measurements Used in the Model Evaluation

Data sets[a]	Parameters[b]	Date frequency	Number of sites	Data sources
ZBAA	T_2, RH_2, WS_{10}, WD_{10}	Daily	1	http://www.wunderground.com
ZBAA	T, RH, WS	08:00, 20:00LST	1	http://weather.uwyo.edu/upperair/sounding.html
CNEMC	O_3, $PM_{2.5}$	Hourly	12	http://113.108.142.147:20035/emcpublish
AERONET	AOD	Hourly	2	https://aeronet.gsfc.nasa.gov/
WRMC-BSRN	SWDOWN	Hourly	1	http://bsrn.awi.de

[a]ZBAA: an international standard weather station at the Beijing Capital International Airport; CNEMC: the China National Environmental Monitoring Center; AERONET: the Aerosol Robotic Network; WRMC-BSRN: the World Radiation Monitoring Center-Baseline Surface Radiation Network. [b]T_2: temperature at 2 m; RH_2: relative humidity at 2 m; WS_{10}: wind speed at 10 m; WD_{10}: wind direction at 10 m; AOD: aerosol optical depth; SWDOWN: shortwave downward radiation flux.

3. Model Configuration

3.1. WRF-Chem Model

The WRF Model version 3.7 (Skamarock et al., 2008) coupled with Chemistry (Grell et al., 2005) is employed to investigate the impacts of urbanization on boundary layer meteorology and air quality over the Beijing metropolitan region. WRF-Chem is configured with three nested domains (Figure 1) using 63 × 53, 70 × 70, and 73 × 73 grid points at 27, 9, and 3-km horizontal resolution, respectively. The first domain covers nearly all the Northern China and the regions of Huanghai and Bohai Sea Circle. Beijing is set to be the center of the innermost nested domain. In order to minimize the influence from lateral boundary conditions, simulation results in the inner region of the third domain (39.41°N–41.18°N, 115.19°E–117.52°E) with 68 × 68 grid points are selected to analyze following Wu et al. (2012) and Chen, Zhang, Zhu, et al. (2017). The vertical grid contains 29 full sigma levels from the surface to 50 hPa, of which the lowest 12 layers are below 1 km for finer resolution in the planetary boundary layer, and the first layer is approximately 16 m.

The initial and lateral boundary conditions of meteorological fields are obtained from the National Center for Environmental Prediction Final Analysis data with 1° × 1° spatial resolution and 6-hr temporal intervals. Four-dimensional data assimilation (FDDA; Otte, 2008) with a nudging coefficient of 3.0×10^{-4} for the

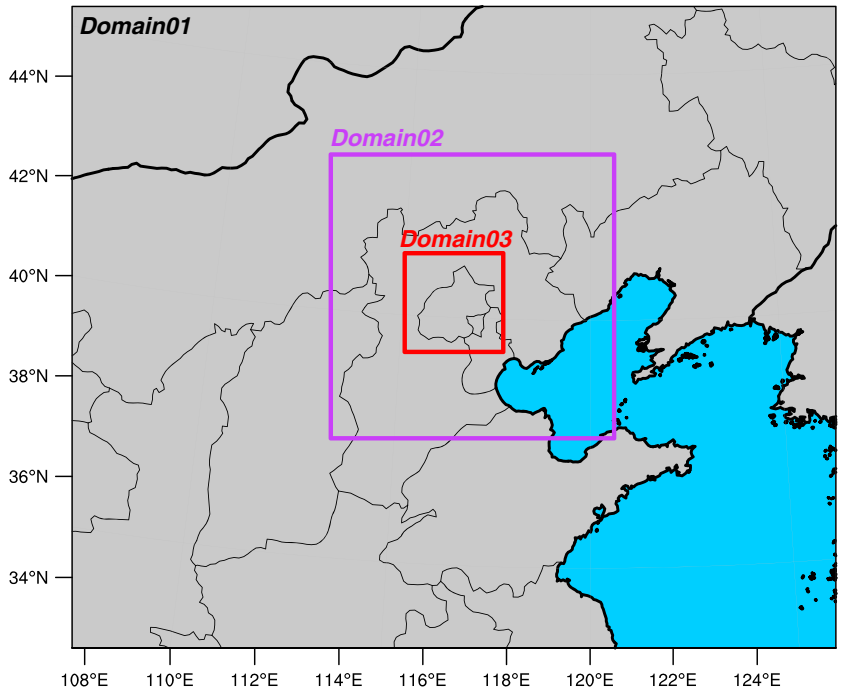

Figure 1. The configuration of the three two-way nested domains for the Weather Research and Forecasting-Chem simulation.

Table 2
Options in the WRF-Chem Model Used in This Study

Options	WRF-Chem
Microphysics option	Purdue Lin scheme
Longwave radiation option	RRTMG scheme
Shortwave radiation option	RRTMG scheme
Surface layer option	Revised MM5 Monin-Obukhov scheme
Land surface option	Unified Noah land surface model
Urban canopy model	Single-layer UCM scheme
Boundary layer option	YSU scheme
Cumulus option	Grell 3-D ensemble scheme
Photolysis scheme	Fast-J
Dust scheme	Shao_2004
Chemistry option	Carbon bond mechanism
Aerosol option	Model for Simulating Aerosol Interactions and Chemistry
Analysis nudging	On (including gird nudging and surface nudging)

temperature, humidity, and wind at all levels is adopted in WRF-Chem model to reduce the model bias of simulated meteorological fields (Lo et al., 2008). The output data from a global chemical transport model MOZART-4 are used as the chemical initial and boundary conditions (Emmons et al., 2010).

The gas-phase chemical mechanism carbon bond mechanism (Zaveri & Peters, 1999) coupled with an 8-bin sectional aerosol model, Model for Simulating Aerosol Interactions and Chemistry (Zaveri et al., 2008), with aqueous chemistry is used in this study. The aerosol size distribution is divided into discrete size bins defined by their lower and upper dry particle diameters (Gao et al., 2015). All major aerosol species are considered in this model, including sulfate, nitrate, ammonium, chloride, sodium, black carbon, primary organic mass, liquid water, and other inorganic mass (Zaveri et al., 2008). The sophisticated Noah land surface scheme developed by Chen et al. (1996) is used to describe the land-atmosphere interactions, which incorporates detailed land surface process of thermodynamics and hydrology, such as vegetation evapotranspiration, soil runoff, and moisture diffusion. The SLUCM (Kusaka et al., 2001; Kusaka & Kimura, 2004) is used to represent the thermal and dynamic effects of urban grids. SLUCM recognizes three-dimensional natures of urban surfaces (roof, wall, and road). The shadowing, reflections, and trapping of radiation are also considered (Chen et al., 2011). Anthropogenic heat (AH), treated as one part of the sensible heat flux in SLUCM (Chen et al., 2011), is included in our study and the AH is characterized by a diurnal cycle with two peaks at rush hours of 08:00 and 17:00 (LST). The maximum value of AH is set to be 90 W m^{-2} following Zhang et al. (2013) and Chen et al. (2016). Detailed parameterization schemes used in this study are listed in Table 2.

3.2. Emissions

The anthropogenic emissions are taken from the monthly 2010 Multi-resolution Emission Inventory for China (http://www.meicmodel.org/). The inventory includes species of sulfur dioxide (SO_2), nitrogen oxides (NO_x), carbon monoxide (CO), carbon dioxide (CO_2), nonmethane volatile organic compounds, ammonia (NH_3), black carbon, organic carbon, $PM_{2.5}$, and PM_{10}. The emissions of all species include four sectors (power, industry, residential, and transportation). The biogenic emissions are calculated online using the Model of Emission of Gases and Aerosol from Nature (Guenther et al., 2006). The biomass burning emissions are taken from the Global Fire Emissions Database (Randerson et al., 2005). Dust emission is calculated using the algorithm proposed by Shao (2004), and sea salt emission is calculated online following Gong et al. (1997).

3.3. Numerical Experiments

To examine the effects of urbanization over Beijing, we perform four simulations with four different land use scenarios for Beijing (Table 3). The CTL case represents current urban situation, in which the land use condition is based on high-resolution Moderate Resolution Imaging Spectroradiometer satellite observation data (Figure 2a). Same as CTL, but all urban grids are replaced by irrigated cropland in the NOURB case (Figure 2b). Irrigate cropland is the most common land cover type in and around Beijing and is often used to represent the preurbanization land cover type (Wang et al., 2012, 2014). In the United States Geological Survey (USGS) case (Figure 2c), the urban areas from USGS land use types are used, while the other land uses remain the same as NOURB. The USGS land use types are based on 1992–1993 1-km Advanced Very High Resolution Radiometer data. A future (year 2050) urban form of Beijing, referred to as COMPACT case (Figure 2d), is also designed following Yang et al. (2016). In the COMPACT case, Beijing is an ideal monocentric city, and the number of urban grids is doubled compared with that in the CTL case. The added urban coverage is distributed around the old urban core region of the CTL case.

Table 3
Experimental Design

Case	Urban scenario	Urban albedo
CTL	Moderate Resolution Imaging Spectroradiometer (MODIS) urban	0.2
NOURB	No urban	0.2
USGS	United States Geological Survey (USGS) urban	0.2
COMPACT	Compact urban	0.2
ALBEDO	MODIS urban	0.85

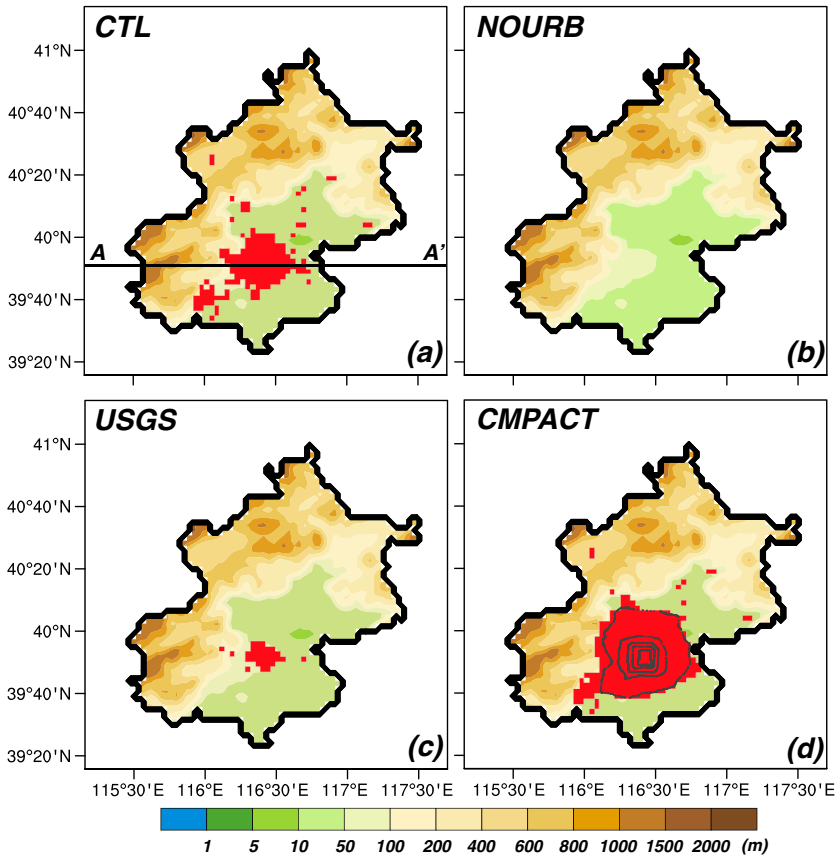

Figure 2. The spatial distribution of Beijing urban grids marked in red for (a) CTL, (b) NOURB, (c) USGS, and (d) COMPACT simulations. Line AA′ in (a) denotes the cross section across the city belt in the Beijing metropolitan area. The black circles in (d) represent the five ring roads. Terrain height is shown by the colored shading (m).

To examine the impacts of UHI mitigation (increasing urban albedo) on air quality, another simulation (referred to as ALBEDO case) is designed, with albedo of roofs, walls, and roads within all urban grids increasing from 0.2 to 0.85, following Wang et al. (2013). The albedo of 0.85 represents an ideal highly reflective white paint (Fallmann et al., 2016).

All the physical and chemical schemes and the emission inventory are the same in these cases. The impacts of urbanization on boundary layer meteorological parameters and air pollutant concentrations can be quantified by comparing the simulation results of CTL, NOURB, USGS, and COMPACT cases. The differences between ALBEDO and CTL simulations represent the effects of increasing urban albedo.

In order to match the periods when observation data are available, our simulations are conducted for the periods from 26 June to 31 July 2015 and 16 November to 21 December 2015, by reinitializing meteorological conditions every 15 days with National Center for Environmental Prediction Final Analysis data and including an overlap period of 5 days for each simulation block as model spin up to minimize the effects of the initial condition. The results from CTL case during 1 to 30 July 2015 (as summer) and 21 November to 20 December 2015 (as winter) are used to compare with observations for model evaluation.

4. Results

4.1. Model Evaluation

4.1.1. Meteorology

Figure 3 shows the time series of observed and simulated daily averaged 2-m temperature (T_2), 2-m relative humidity (RH_2), 10-m wind speed (WS_{10}), and 10-m wind direction (WD_{10}) at ZBAA station during 1 to 30 July 2015 (as summer, a1–d1) and 21 November to 20 December 2015 (as winter, a2–d2). The corresponding

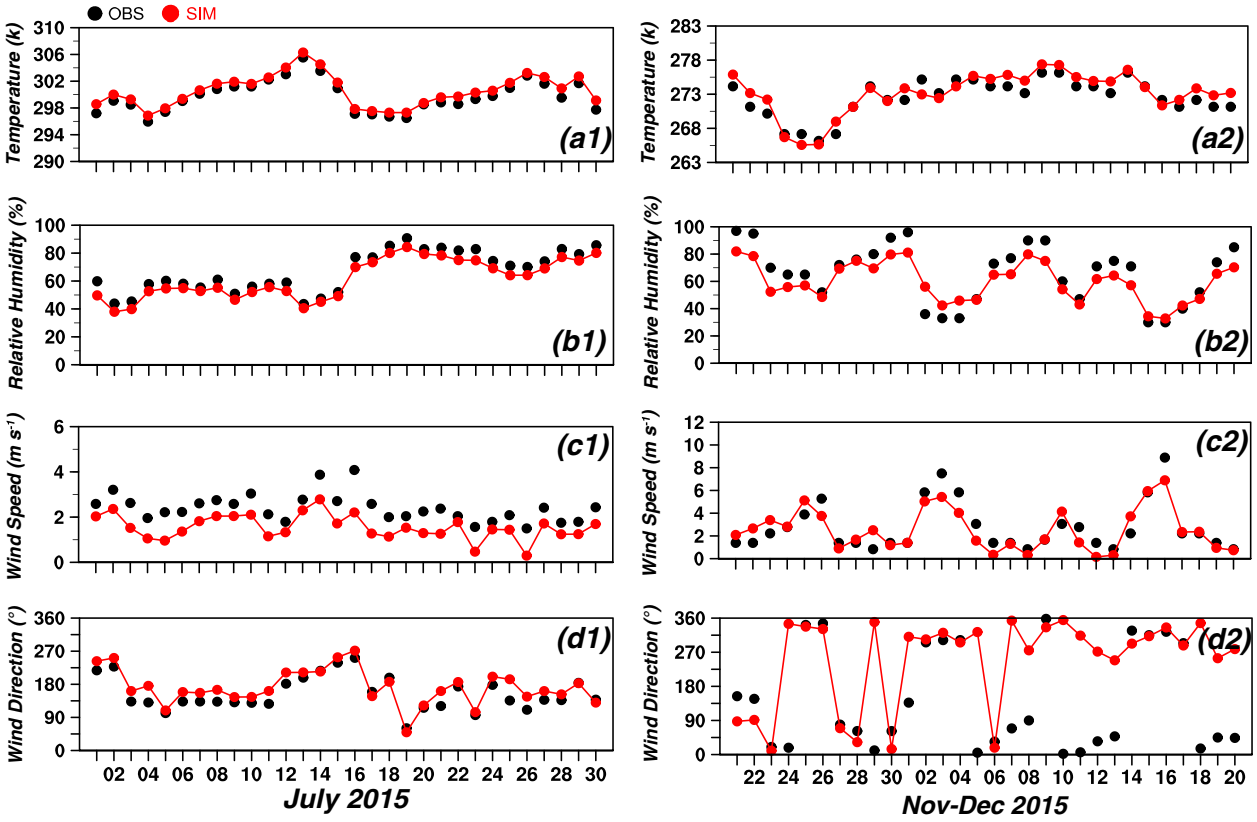

Figure 3. Time series of observed (in black dots) and simulated (in red dots) daily 2-m temperature (k), 2-m relative humidity (%), 10-m wind speed (m s^{-1}), and 10-m wind direction (°) at the ZBAA station during 1 to 30 July 2015 (a1–d1) and 21 November to 20 December 2015 (a2–d2).

statistical metrics, including mean bias (MB), root mean square error (RMSE), and correlation coefficient (*R*), are listed in Table 4.

As shown in Figure 3, the simulated meteorological variables agree well with observations. For temperature, the WRF-Chem model almost perfectly reproduces the high values in summer and low values in winter, with high Rs of 0.97 in summer and 0.92 in winter. Both MBs are less than 1 °C. For relative humidity, the model captures the temporal variations fairly well, with Rs of 0.92 in summer and 0.94 in winter, but underestimates the observed values with MBs of −5.1% in summer and −5.9% in winter. Qian et al. (2016) pointed out that different planetary boundary layer and surface parameterizations had large impacts on surface moisture fluxes and that the setting of the schemes could result in the mismatch of relative humidity between observations and simulations. The bias of relative humidity can also be found in other studies (Gao et al., 2015; Zhang et al., 2009). Generally, the simulated wind speed agrees well with the measurements with Rs lager than 0.8. But the model underestimates the wind speed both in summer (MB is −0.84 m s^{-1}) and in winter (MB is −0.21 m s^{-1}). This underestimation may be caused by the inaccurate land surface characteristics we used in this study. The simulated wind directions in summer agree well with observations with *R* of 0.93, MB of +17.8°, and RMSE of 24.6°. However, a large deviation can be found in winter, especially for the northerly winds (north-northwest winds from simulation versus north-northeast winds from observation), which may be attributed to the coarse model resolution.

Observed and simulated vertical profiles of temperature, relative humidity, and wind speed from ZBAA station at 08:00 and 20:00 (LST) averaged over summer and winter are also shown in Figures S2 and S3. Generally, the model captures the vertical profiles of temperature quite well both in summer and winter. However, the performance of relative humidity and wind speed is not as good as that of temperature. Overestimation of relative humidity and underestimation of wind speed are found both in summer and winter.

Table 4
Statistics for the Observed and Simulated 2-m Temperature (Temp, k), 2-m Relative Humidity (RH, %), 10-m Wind Speed (WS, m s^{-1}), 10-m Wind Direction (WD, °), Surface O_3 (ppbv), and $PM_{2.5}$ ($\mu g\ m^{-3}$) Concentrations During 1 to 30 July 2015 (as Summer) and 21 November to 20 December 2015 (as Winter)

	Summer					Winter				
Variables	$\overline{OBS}$[d]	$\overline{SIM}$[d]	MB[a]	RMSE[b]	R[c]	$\overline{OBS}$[d]	$\overline{SIM}$[d]	MB[a]	RMSE[b]	R[c]
Temp (k)	299.8	300.6	0.79	0.85	0.97	272.5	273.2	0.66	1.4	0.92
RH (%)	66.9	61.8	−5.1	5.4	0.92	65.8	59.9	−5.9	10.7	0.94
WS (m s^{-1})	2.39	1.56	−0.84	0.90	0.83	2.75	2.54	−0.21	1.1	0.87
WD (°)	154.4	172.2	17.8	24.6	0.93	143	250.1	107.1	183.1	0.31
O_3 (ppbV)	48.2	56.9	8.7	11.8	0.84	9.1	11.1	2.0	3.6	0.90
$PM_{2.5}$ ($\mu g\ m^{-3}$)	62.0	68.4	6.4	19.8	0.80	120	121.7	1.6	40.3	0.93

Note. Where SIM_i and OBS_i indicate the predicted and observed parameter, respectively. *i* refers to a given time, and nstd is the total number of samples.
[a]Mean bias, $MB = \sum_{i=1}^{nstd}(SIM_i - OBS_i)/nstd$. [b]Root mean square error, $RMSE = \sqrt{\sum_{i=1}^{nstd}(SIM_i - OBS_i)^2/nstd}$. [c]Correlation coefficient, $R = \frac{\sum_i^{nstd}\left|(OBS_i - \overline{OBS}) \times (SIM_i - \overline{SIM})\right|}{\sqrt{\sum_i^{nstd}(OBS_i - \overline{OBS})^2 + \sum_i^{nstd}(SIM_i - \overline{SIM})^2}}$. [d]$\overline{OBS} = \frac{1}{nstd} \times \sum_1^{nstd} OBS_i$, $\overline{SIM} = \frac{1}{nstd} \times \sum_1^{nstd} SIM_i$.

4.1.2. Particle Matter and Gas-Phase Pollutants

Figure 4 shows the time series of observed and simulated daily surface-layer O_3 and $PM_{2.5}$ concentrations during 1 to 30 July 2015 (as summer, a1–b1) and 21 November to 20 December 2015 (as winter, a2–b2). The observations are averaged among the 12 stations in Beijing (1001A–1012A), and the model results are from CTL case. Daily O_3 and $PM_{2.5}$ concentrations at each station are shown in Figures S3–S6. The statistical parameters are listed in Table 4.

In general, the WRF-Chem model reasonably reproduces the magnitudes and variations of observed surface-layer O_3 ($PM_{2.5}$) concentrations both in summer and winter, with RMSEs of 11.8 ppbv (19.8 $\mu g\ m^{-3}$) in summer and 3.6 ppbv (40.3 $\mu g\ m^{-3}$) in winter, and Rs of 0.84 (0.8) in summer and 0.9 (0.93) in winter. However, the model underestimates the peak values of $PM_{2.5}$ concentrations in winter, especially during the heavy polluted period from 27 November to 1 December 2015. The underestimation can be found at nearly all the 12 stations (Figure S7), which is partly attributed to the outdated emission inventory. What is more, the negative bias of relative humidity may also account for underestimation of aerosol concentrations during fog-haze event in winter (Mölders et al., 2012).

4.1.3. Aerosol Optical Depth

Figure 5 shows the scatterplots of hourly AOD values at 550 nm taken from AERONET and CTL case for two sites (Beijing and Beijing_CAMS) during 1 to 30 July 2015 (as summer, a1–b1) and 21 November to 20 December 2015 (as winter, a2–b2).

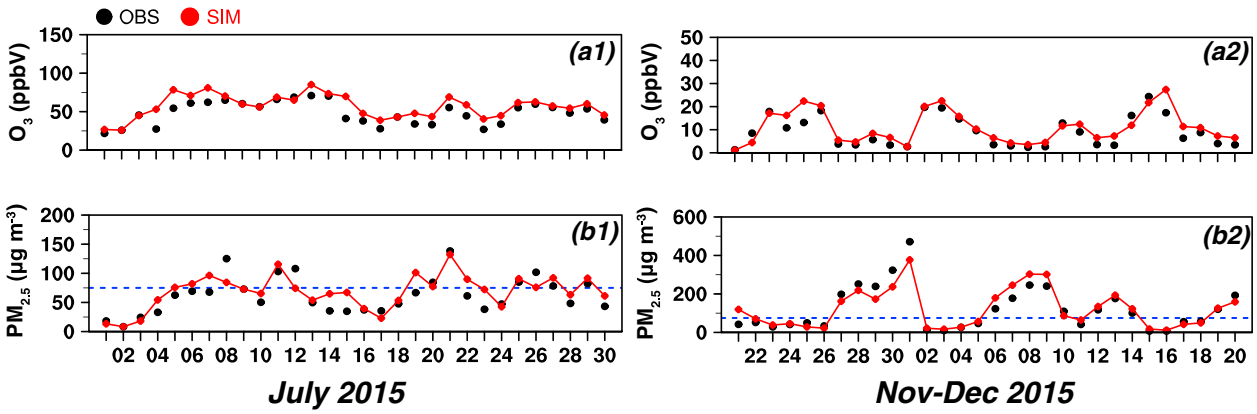

Figure 4. Time series of observed (in black dots) and simulated (in red dots) daily O_3 (ppbv) and $PM_{2.5}$ ($\mu g\ m^{-3}$) concentrations averaged among the 12 stations in Beijing (1001A–1012A) during 1 to 30 July 2015 (a1–b1) and 21 November to 20 December 2015 (a2–b2).

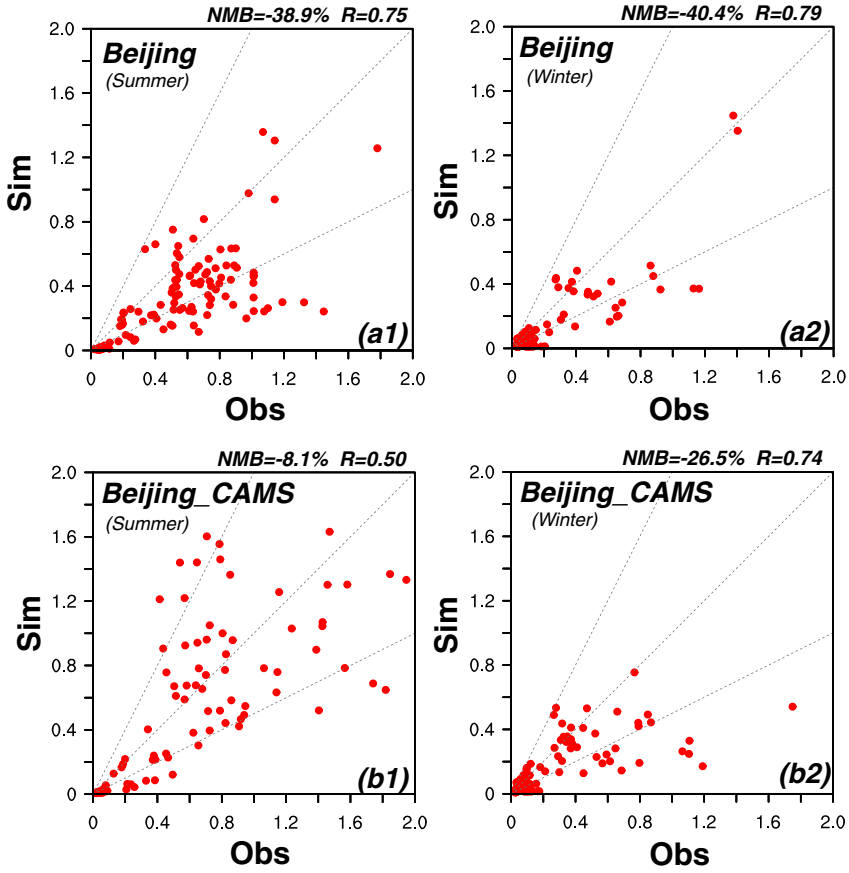

Figure 5. Scatterplots of the observed and simulated hourly aerosol optical depth (AOD) at Beijing and Beijing_CAMS sites during 1 to 30 July 2015 (a1–b1) and 21 November to 20 December 2015 (a2–b2). Also shown in panels are the 1:1, 1:2, and 2:1 lines (dashed). The normalized mean bias and the correlation coefficient between simulated and observed AOD are shown on the top right corner of each panel.

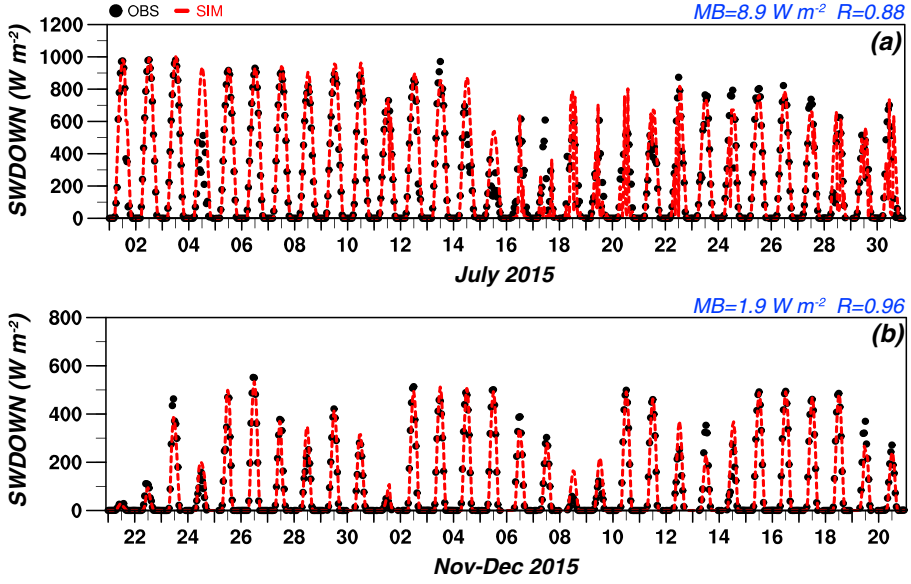

Figure 6. Time series of observed (in black dots) and simulated (in red dash lines) hourly shortwave downward radiation flux (SWDOWN) at the Xianghe station during (a) 1 to 30 July 2015 and (b) 21 November to 20 December 2015. The mean bias and the correlation coefficient between simulated and observed SWDOWN are shown on the top right corner of each panel. Unit: W m^{-2}.

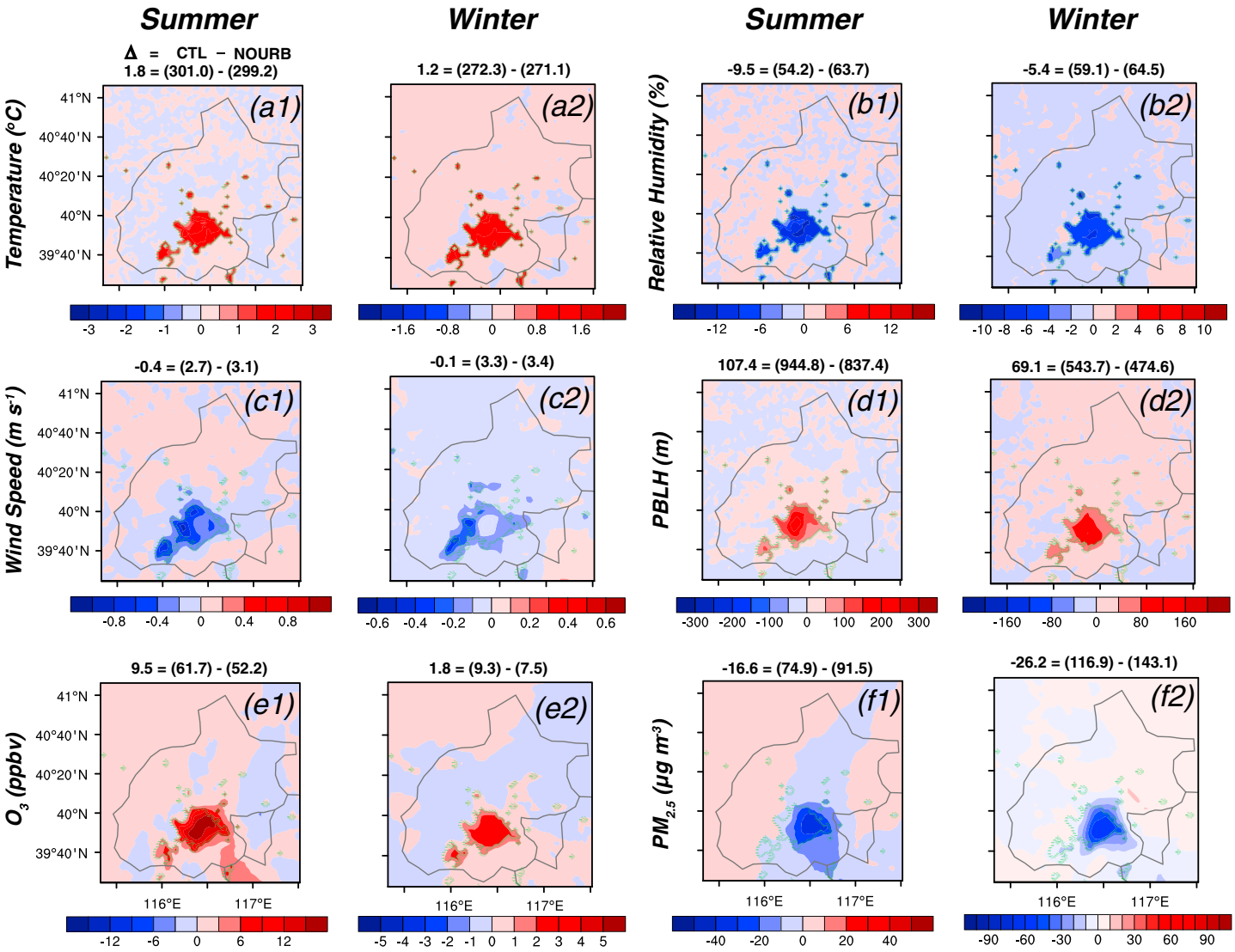

Figure 7. The differences in T_2 (°C), RH_2 (%), WS_{10} (m s^{-1}), planetary boundary layer height (m), surface O_3 (ppbv), and $PM_{2.5}$ (μg m^{-3}) concentrations between CTL and NOURB simulations (CTL minus NOURB) averaged during 1 to 30 July 2015 (as summer, a1–f1) and 21 November to 20 December 2015 (as winter, a2–f2). The urban area of Beijing is marked by the green lines. Mean values from CTL and NOURB simulations and their differences averaged over the urban grids are shown above each panel.

The WRF-Chem model generally reproduces the observed AOD values within a factor of 2. The Rs between observations and simulations are in the range of 0.5–0.79. The normalized MBs are negative (from −40.4% to −8.1%), indicating the underestimation of simulated AOD at both stations. The underestimation can also be found in other studies (Gao et al., 2015; Hu et al., 2016). The coarse-resolution (inner) setting and inaccurate anthropogenic aerosol emission may lead to this underestimation.

4.1.4. Radiation

In order to evaluate the surface energy budget, simulated hourly shortwave (SW) downward radiation flux is compared with observations at the Xianghe radiometric station (Figure 6). The simulation results from CTL case agree well with the observed values, not only the daily maximum but also the small values when weather phenomena occurred, such as the heavy fog-haze event happened in 1 December 2015. The MBs are 8.9 W m^{-2} in summer and 1.9 W m^{-2} in winter; the Rs are 0.88 in summer and 0.96 in winter.

In summary, WRF-Chem model reproduces the spatial-temporal evolutions of both meteorological and chemical variables fairly well, which provides confidence for further investigation.

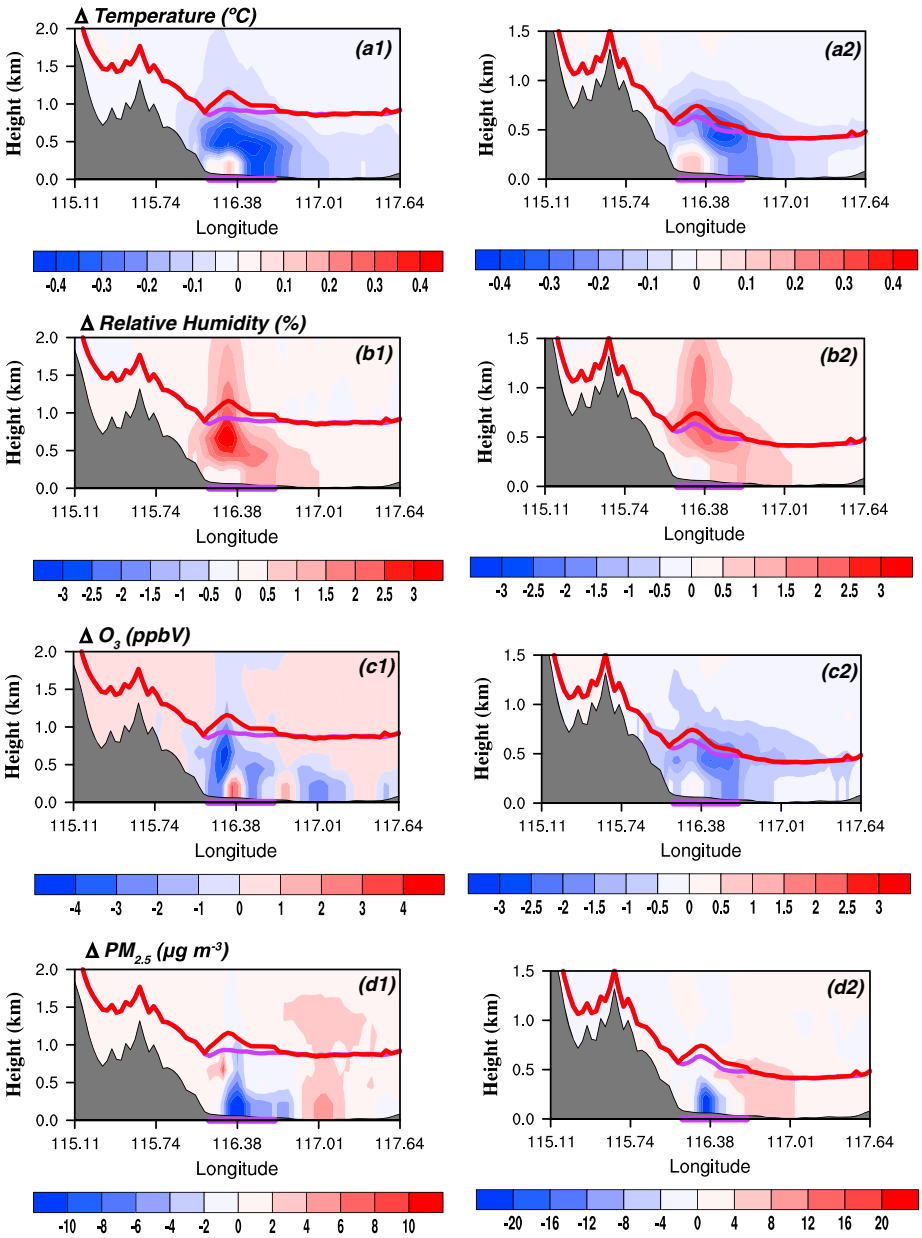

Figure 8. Cross sections of differences in temperature (°C), relative humidity (%), O_3 (ppbv), and $PM_{2.5}$ (μg m^{-3}) between CTL and NOURB cases along AA′ (marked in Figure 2a) averaged during 1 to 30 July 2015 (a1–d1) and 21 November to 20 December 2015 (a2–d2). The planetary boundary layer height simulated by CTL (in red line) and NOURB (in purple line) is also shown in each panel. The thick purple bar along the horizontal ordinate represents the extent of urban areas, and the black-shaded areas represent terrain.

4.2. Impacts of Urbanization on Meteorology and Air Quality

Urbanization is considered as an irreversible process. Rapid changes in land cover during urban sprawl can modify the surface properties, such as urban surface albedo, and then have significant impacts on boundary layer meteorology and air quality. Figure 7 shows the differences in T_2, RH_2, WS_{10}, PBLH, surface O_3, and $PM_{2.5}$ concentrations between CTL and NOURB cases (CTL minus NOURB, representing the impacts of urban sprawl) averaged in summer and winter. Due to increased heat capacity and decreased surface albedo induced by urbanization, T_2 is increased by 1.8 °C in summer and 1.2 °C in winter averaged over the urban grids, and the warming areas are concentrated in the center of the highly urbanized region. More solar

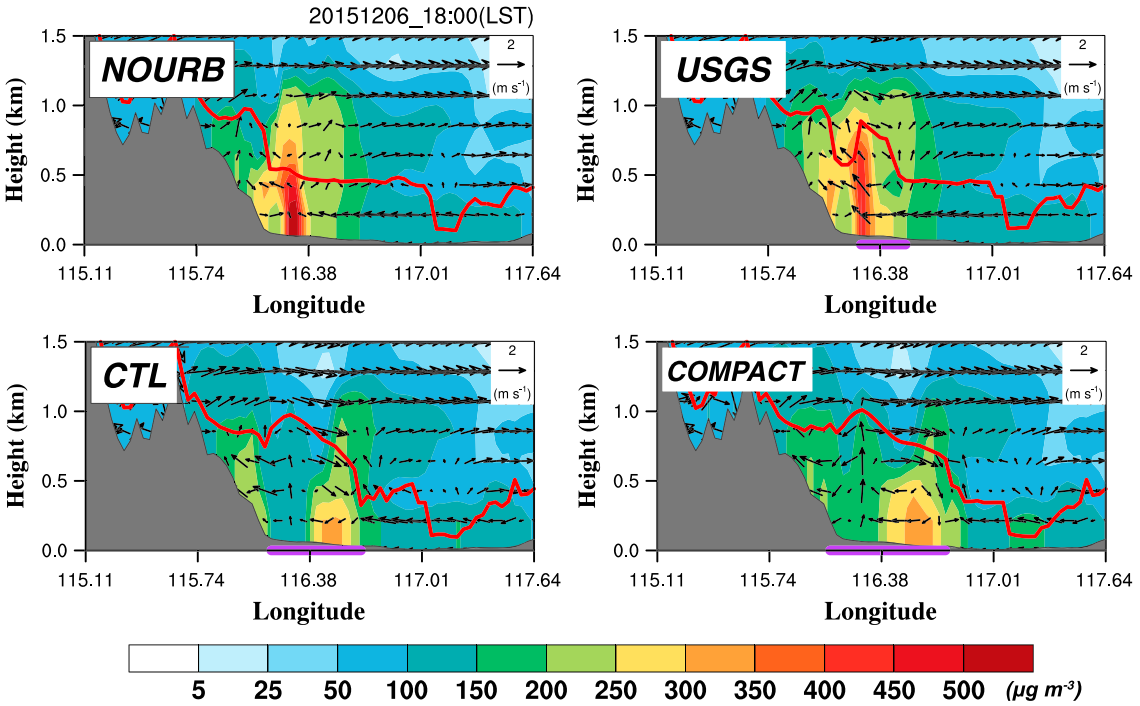

Figure 9. Cross sections of $PM_{2.5}$ concentrations (μg m^{-3}, in colored shading) and wind fields (m s^{-1}, in black arrows) from (a) NOURB, (b) USGS, (c) CTL, and (d) COMPACT simulations along AA′ (marked in Figure 2a) at 18:00 (LST) on 6 December 2015. The planetary boundary layer height simulated by each case is also shown in each panel (red line). The thick purple bar along the horizontal ordinate represents the extent of urban areas in each simulation. The black-shaded areas represent terrain. Note that the vertical velocity is multiplied by a factor of 10 when plotting wind vectors.

radiation absorbed and trapped in the urban canopy in summer can explain the larger increase in T_2 during summer than that during winter. Urban sprawl changes land cover from natural land surface to impervious concrete surface, and therefore, less water is available for evaporation in urbanized areas, which makes RH_2 decrease by 9.5% in summer and 5.4% in winter. Urbanization can also increase the surface roughness owing to the friction effect of tall buildings. The dragging force makes the near surface wind speed in urban areas decrease, with the magnitude of −0.4 m s^{-1} in summer and −0.1 m s^{-1} in winter. Urbanization increases the PBLH by 107.4 m in summer and 69.1 m in winter. The larger increase in PBLH in summer may be attributed to the larger increase in T_2. The surface-layer O_3 concentration is increased both in summer (+9.5 ppbv) and winter (+1.8 ppbv). The increased air temperature accelerates O_3 formation by increasing its reaction rate. Meanwhile, the decreased wind speed suppresses O_3 transport and facilitates O_3 accumulation in urban areas. The $PM_{2.5}$ concentration is decreased by 16.6 μg m^{-3} in summer and 26.2 μg m^{-3} in winter, respectively. Although urban sprawl makes the wind speed in urbanized areas reduced which is unfavorable for transport, the increased PBLH may dilute and disperse the surface-layer $PM_{2.5}$ concentrations.

Cross sections of differences in temperature, relative humidity, O_3, and $PM_{2.5}$ between CTL and NOURB cases averaged in summer and winter are shown in Figure 8. Urban sprawl increases the near-surface air temperature in urban areas but decreases it at the higher altitudes (400–1,000 m) both in summer and winter. The changes in relative humidity are contrary to those of temperature, with the maximum increase above the height of 500 m. The changes in air temperature can directly influence the rate of O_3 formation (Li et al., 2016; Liao et al., 2015). Therefore, the patterns in O_3 differences are similar to those in temperature changes in the boundary layer. Urban sprawl decreases the $PM_{2.5}$ concentrations over the urbanized areas, and the reduction is found from the surface up to the height of 500 m. However, the $PM_{2.5}$ concentrations exhibit increases in rural areas both in summer and winter, with the magnitude of 6 μg m^{-3}.

To explain the increase in $PM_{2.5}$ concentrations over rural areas, we show cross sections of simulated $PM_{2.5}$ concentrations and wind fields from the four cases (NOURB, USGS, CTL, and COMPACT) at 18:00 LST on 6

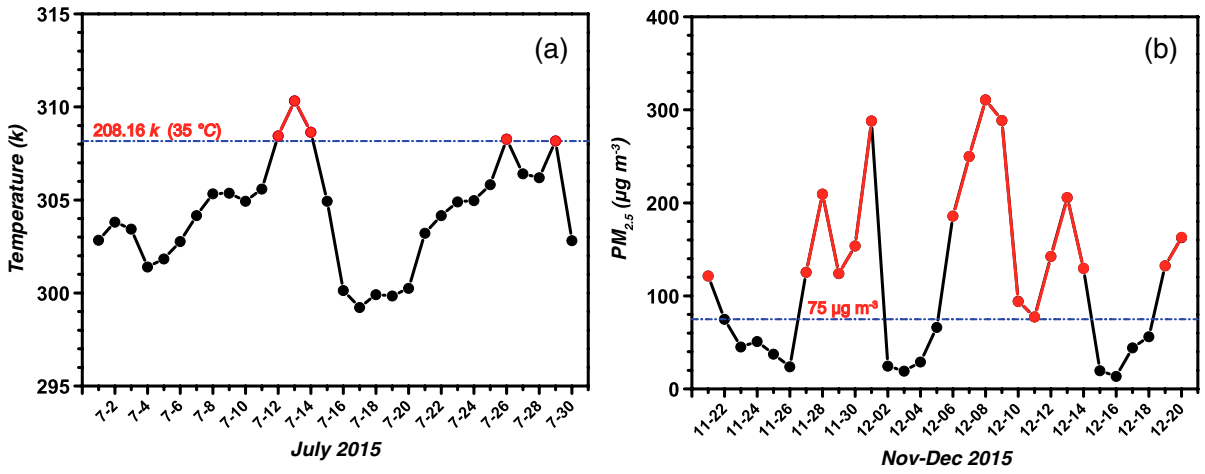

Figure 10. Time series of simulated daily (a) near-surface air temperature (k) during 1 to 30 July 2015 and (b) surface $PM_{2.5}$ concentration (μg m^{-3}) during 21 November to 20 December 2015 averaged over the Beijing urban areas. The red dots in (a) and (b) represent the hot days and the polluted days, respectively.

December 2015 in Figure 9. From NOURB to USGS, and further to CTL and COMPACT, the urban areas are significantly expanded. Urban sprawl changes natural landscape into impervious surface, which increases the heat capacity and heat storage and makes more solar radiation absorbed in urban areas. After sunset, more heat flux is released from the urban canopy, and therefore, the lower urban atmosphere becomes warmer than surrounding rural areas. Because of the enhanced urban turbulent mixing and upward transport by the rising branch of UHI circulation, more aerosol particles in urban areas are carried to the upper atmosphere (>1 km), which reduces the surface-layer $PM_{2.5}$ concentrations in urban areas. Parts of the lifted aerosol particles are transported to downwind areas by upper-level westerly wind; some are accumulated around the urban-rural borders by the sinking branch of UHI circulation. The trapped $PM_{2.5}$ at the suburban region may not only worsen the air quality in rural areas but also further exacerbate air quality in urban areas through aerosol particle recirculation by the surface UHI convergence.

To better understand the effects of urbanization on boundary layer meteorology and air quality over Beijing under different weather conditions, we highlight HW days in summer and polluted days in winter in Figure 10. In summer, a day with the daily mean temperature averaged over the urban areas in Beijing larger than 35 °C is defined as an HW day (Smith et al., 2013; Tan et al., 2007). In winter, a day with the daily mean $PM_{2.5}$ concentration averaged over the urban areas in Beijing larger than 75 μg m^{-3} is classified as a polluted day (see the Grade II standard defined by the National Ambient Air Quality Standards of China).

Table 5 shows the impacts of urbanization on meteorological and chemical parameters averaged over the Beijing urban areas under different weather conditions. In summer, the UHI intensity, quantified by the difference in urban-rural temperature, is enhanced by 11.1% (from 1.8 °C in normal days to 2.0 °C during HWs).

Table 5
The Impacts of Urbanization on 2-m Temperature (Temp, k), 2-m Relative Humidity (RH, %), PBLH (m), Surface O_3 (ppbv), and $PM_{2.5}$ (μg m^{-3}) Concentrations Averaged Over the Beijing Urban Areas

Period	Weather Condition	Temp (k)			RH (%)			PBLH (m)			O_3 (ppbv)			$PM_{2.5}$ (μg m^{-3})		
		CTL[a]	NOURB[b]	Delta[c]	CTL	NOURB	Delta	CTL	NOURB	Delta	CTL	NOURB	Delta	CTL	NOURB	Delta
Summer (1 to 30 July 2015)	BG[d]	303.4	301.6	1.8	55.6	65.3	−9.6	922.4	815.7	106.7	59.5	49.7	9.8	75.1	91.5	−16.3
	HW[d]	308.8	306.8	2.0	41.0	49.2	−8.3	1146.3	1033.1	113.3	81.9	75.0	7.0	72.5	91.8	−19.4
Winter (21 November to 20 December 2015)	AQS1[e]	271.0	269.8	1.2	46.2	54.6	−8.4	757.4	667.8	89.5	19.1	15.5	3.5	21.7	27.5	−5.8
	AQS2[e]	273.6	272.1	1.4	65.9	71.4	−5.5	456.5	389.8	66.7	5.2	3.9	1.3	176.6	216.1	−39.5

[a]Parameters simulated by CTL case averaged over the urban grids. [b]Parameters simulated by NOURB case averaged over the corresponding urban grids in CTL case. [c]The differences between CTL and NORUB simulations (CTL minus NORUB). [d]BG and HW are defined in Figure 12. [e]AQS1 and AQS2 are defined in Figure 11.

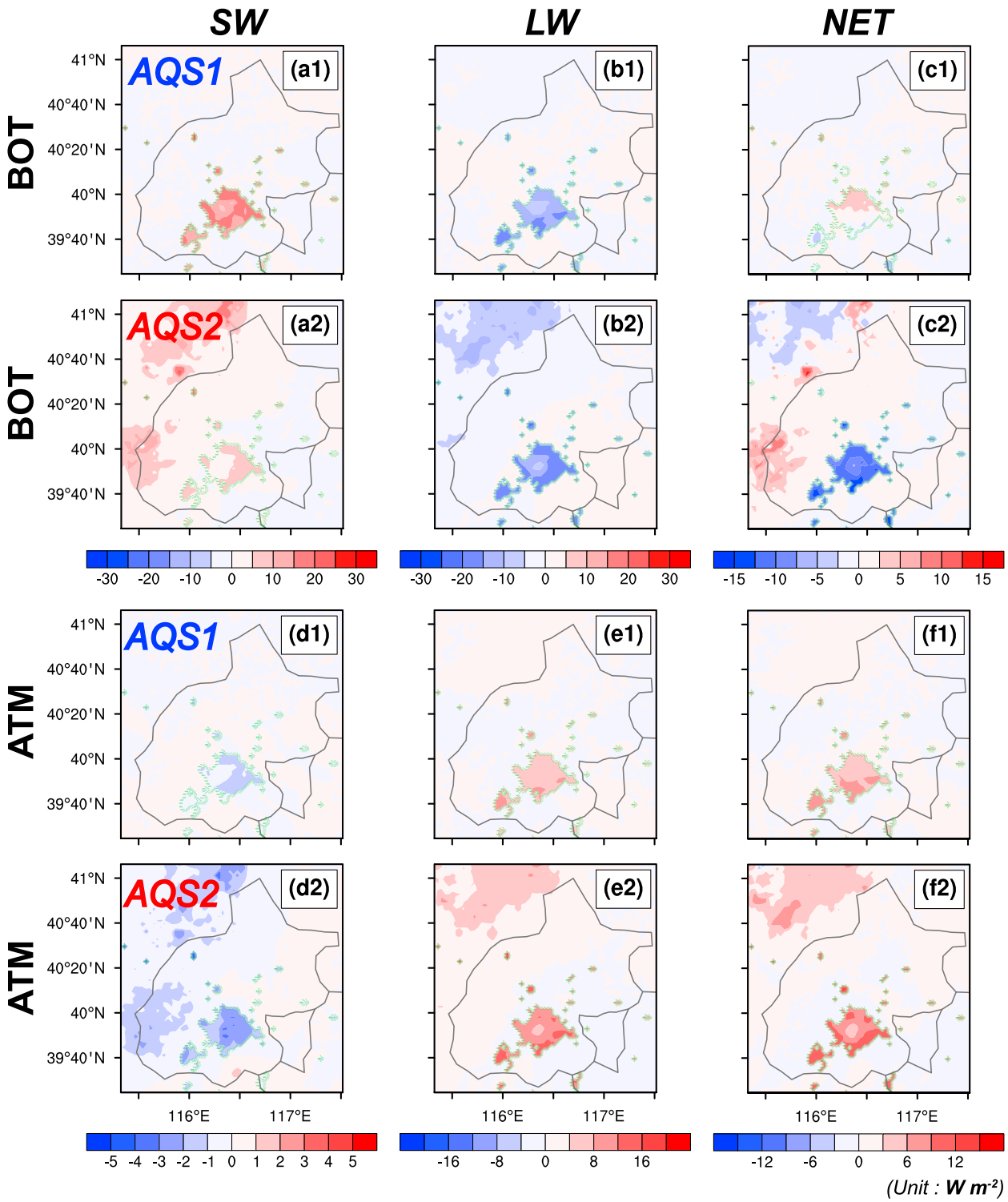

Figure 11. The differences in simulated all-sky radiative forcing between CTL and NOURB cases averaged during 21 November to 20 December 2015. AQS1 denotes the clean days with the daily mean surface $PM_{2.5}$ concentration averaged over the Beijing urban areas less than 75 μg m^{-3}, while AQS2 represents the polluted days with the $PM_{2.5}$ concentration larger than 75 μg m^{-3}. "BOT" and "ATM" denote the radiative forcing at the surface and in the atmosphere, respectively. "NET" denotes the sum of shortwave (SW) and longwave (LW) radiative forcing. Unit: W m^{-2}.

Table 6
The Differences in Simulated Radiative Forcing Between CTL and NOURB Cases (CTL Minus NOURB) Averaged Over the Beijing Urban Areas During 21 November to 20 December 2015 Under Different Weather Conditions

	SW[a] Radiation			LW[a] Radiation			NET[a] Radiation		
	AQS1[a]	ASQ2[a]	Avg[b]	AQS1	AQS2	Avg	AQS1	AQS2	Avg
BOT[a]	14.9[a]	5.6	8.2	−13.7	−16.4	−15.1	1.2	−10.8	−6.9
ATM[a]	−1.0	−2.1	−1.6	6.9	11.5	9.7	5.9	9.4	8.1

Note. Unit: W m^{-2}.
[a]SW, LW, NET, AQS1, AQS2, BOT, and ATM are defined in Figure 11. [b]Avg denotes the mean value averaged during 21 November to 20 December 2015.

The decrease in relative humidity induced by urban sprawl is reduced from 9.6% in normal days to 8.3% under HWs. The increase in PBLH owing to urbanization is larger under HWs (113.3 m) than that in normal days (106.7 m). The impact of urbanization on O_3 concentrations is reduced from +9.8 ppbv in normal days to +7.0 ppbv under HWs. The decreases in $PM_{2.5}$ concentrations induced by urbanization are larger under HWs (19.4 μg m^{-3}) than those in normal days (16.3 μg m^{-3}).

In winter, the UHI intensity is enhanced by 16.7% (from 1.2 °C in clean days to 1.4 °C in polluted days). The decrease in relative humidity induced by urban sprawl is reduced from 8.4% in clean days to 5.5% in polluted days. The increase in PBLH owing to urbanization is smaller in polluted days (66.7 m) than that in clean days (89.5 m). The impact of urbanization on O_3 concentrations is reduced from +3.5 ppbv in clean days to +1.3 ppbv in polluted days. The decreases in $PM_{2.5}$ concentrations induced by urbanization are larger in polluted days (39.5 μg m^{-3}) than those in clean days (5.8 μg m^{-3}).

As discussed above, UHI intensity is enhanced in polluted days during winter. To explain this phenomenon, we show the differences in simulated all-sky radiative forcing (RF) between CTL and NORUB cases averaged during winter in Figure 11. Table 6 lists the changes in RF induced by urbanization averaged over the Beijing urban areas under different weather conditions. At the surface (referred to as BOT), urban sprawl has a positive SW radiative perturbation in urbanized areas due to the radiation trapping effects and reduced surface albedo caused by urbanization. More aerosols absorb and scatter more solar radiation in polluted days; therefore, the SW radiation flux is smaller (14.9 W m^{-2} in clean days versus 5.6 W m^{-2} in polluted days). Urban sprawl significantly increases the surface temperature and therefore more longwave radiation is emitted in the urban areas. The influence of urbanization on the longwave radiation is enhanced from −13.7 W m^{-2} in clean days to −16.4 W m^{-2} in polluted days. Generally, urbanization produces a net warming effect at

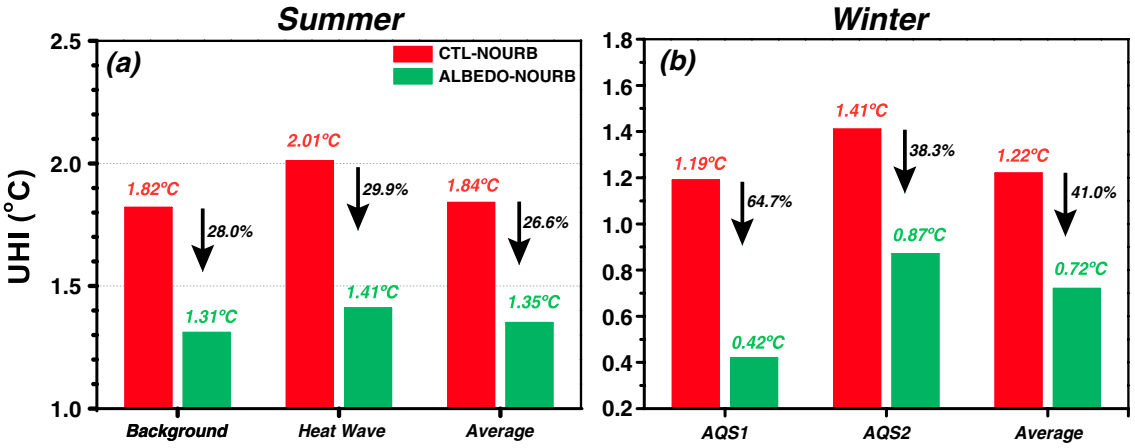

Figure 12. Urban heat island (UHI) intensity (°C) with different urban albedo values under different weather conditions. The red bars and green bars represent UHI intensity with an urban albedo value of 0.2 and 0.85, respectively. In summer, "background" (BG) denotes the normal days when daily mean near-surface air temperature averaged over the Beijing urban areas is less than 35 °C, while "heat wave" (HW) denotes the hot days when the temperature is larger than 35 °C. In winter, AQS1 represents the clean days and AQS2 represents the polluted days, which are defined in Figure 11.

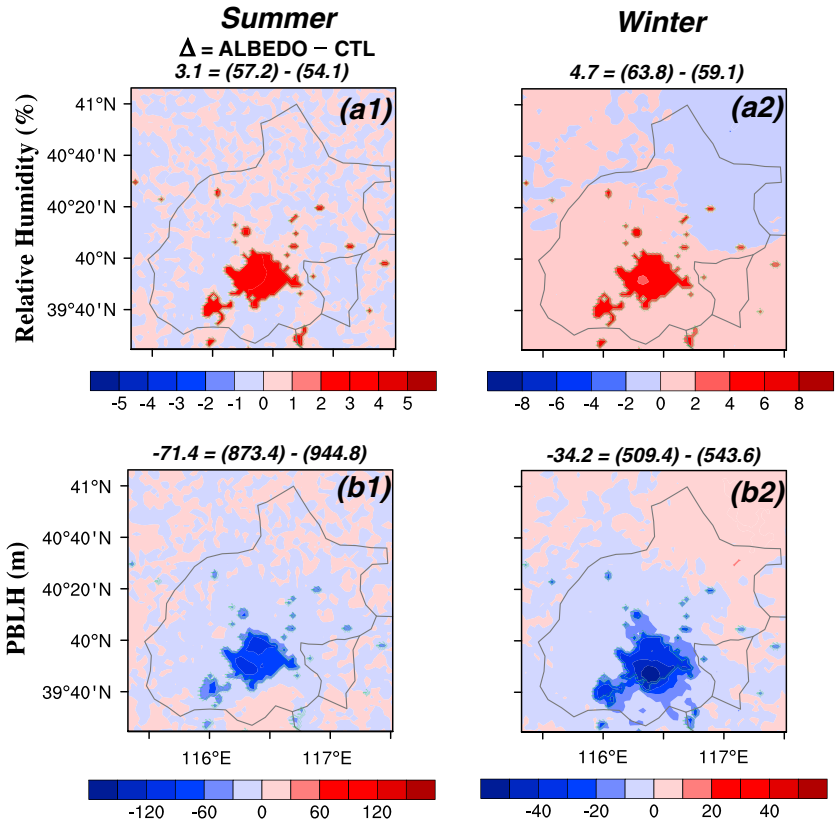

Figure 13. The differences in RH_2 (%) and planetary boundary layer height (m) between ALBEDO and CTL simulations (ALBEDO minus CTL) averaged during 1 to 30 July 2015 (as summer, a1–b1) and 21 November to 20 December 2015 (as winter, a2–b2). The urban area of Beijing is marked by the green lines. Mean values from ALBEDO and CTL simulations and their differences averaged over the urban grids are shown above each panel.

the surface in clean days, with a regional-averaged RF of 1.2 W m^{-2}, while a net cooling effect of −10.8 W m^{-2} is found at the surface during polluted days. This means more radiation is released from the surface and therefore warms the air temperature over urban areas in polluted days, which leads to the enhancement of UHI intensity. This can also be verified by the larger net RF in the atmosphere (9.4 W m^{-2} in polluted days versus 5.9 W m^{-2} in clean days).

4.3. Impacts of Increasing Surface Albedo on Meteorology and Air Quality

Rapid urban expansion significantly increases the air temperature in urban areas and then enhances the UHI intensity, which further affects the thermal comfort of human beings living in urban areas and causes heat-related health problems (Chen et al., 2016). Increasing urban albedo is an effective mitigation strategy to reduce UHI intensity (Touchaei et al., 2016). The cool surfaces and roofs increase the reflection of incoming solar radiation in urban areas and therefore reduce the sensible heat flux and the heat storage available for transmission to the air (Li et al., 2014).

Figure 12 shows the impacts of increasing urban albedo on UHI intensity under different weather conditions. The urban albedo in the CTL case (current urban situation) is set to 0.2. In summer, the UHI intensity is 1.8 °C in normal days and increased to 2.0 °C during HWs. When the albedo of roofs, walls, and roads within all urban grids increase from 0.2 to 0.85 (an ideal highly reflective white paint), the UHI intensity is significantly decreased both in normal days (by 28.0%) and hot days (by 29.9%). In winter, the UHI intensity is increased from 1.2 °C in clean days to 1.4 °C in polluted days. The UHI mitigation by increasing urban albedo is more effective during clean days (by 64.7%) than in polluted days (by 38.3%), indicating that more aerosols may not only enhance the UHI intensity but also weaken the mitigation effects on UHI in winter.

The impacts of increasing surface albedo on relative humidity and PBLH are also analyzed in Figure 13. When the albedo increase from 0.2 to 0.85, the RH_2 is increased by 3.1% in summer and 4.7% in winter averaged

Table 7
Impacts of Increasing Surface Albedo on the Daily Maximum and the Daily Average $PM_{2.5}$ ($\mu g\ m^{-3}$) and O_3 (ppbv) Concentrations Averaged Over the Beijing Urban Areas Under Different Weather Conditions

		Summer (1 to 30 July 2015)						Winter (21 November to 20 December 2015)					
		Daily maximum			Daily average			Daily maximum			Daily average		
Species	Weather condition	ALBEDO	CTL	Delta	ALBEDO	CTL	Delta	ALBEDO	CTL	Delta	ALBEDO	CTL	Delta
$PM_{2.5}(\mu g\ m^{-3})$	Type1[a]	124.2	114.9	9.3	84.5	75.1	9.4	37.1	34.0	3.1	24.6	21.7	2.9
	Type2[b]	140.4	113.4	27.0	89.6	72.5	17.1	200.5	192.1	8.5	184.6	176.6	8.0
	Avg	125.8	114.8	11.1	85.1	74.9	10.2	136.3	128.8	7.5	123.0	116.9	6.1
O_3(ppbV)	Type1[a]	100.0	99.6	0.38	55.9	59.5	−3.5	28.3	31.9	−3.7	16.9	19.1	−2.2
	Type2[b]	156.4	143.7	12.8	80.4	81.9	−1.6	15.6	17.7	−2.2	4.6	5.2	−0.6
	Avg	105.5	103.7	1.8	58.4	61.7	−3.3	19.4	21.9	−2.5	8.3	9.3	−1.0

[a]In summer, Type 1 means normal days. In winter, Type 1 means clean days. [b]In summer, Type 2 means heat wave days. In winter, Type 2 means polluted days.

over the Beijing urban areas. Because more solar radiation is reflected back to the space, turbulent mixing in urban areas becomes weaker and therefore the PBLH is decreased by 71.4 m in summer and 34.2 m in winter.

Increasing urban albedo helps to mitigate UHI effect, and it also has impacts on urban air quality. Table 7 shows the effects of increasing urban albedo on the daily maximum and the daily average $PM_{2.5}$ and O_3 concentrations averaged over the Beijing urban grids under different weather conditions. When the albedo increases from 0.2 to 0.85, both the daily maximum and the daily average surface-layer $PM_{2.5}$ concentrations are increased in summer and winter. The daily average $PM_{2.5}$ concentrations are increased by 10.2 $\mu g\ m^{-3}$ in summer and 6.1 $\mu g\ m^{-3}$ in winter. The increases in surface-layer $PM_{2.5}$ concentrations may be attributed to the decreases in PBLH. Compared with normal days (clean days), the increase in $PM_{2.5}$ concentrations is larger under HWs during summer (in polluted days during winter). The daily mean O_3 concentrations averaged over the Beijing urban areas are decreased both in summer and winter when the urban albedo is increased. However, the daily maximum O_3 concentration in summer is increased, and the increase is larger under HWs (12.8 ppbv) than in normal days (0.38 ppbv), mainly due to the high intensity of reflected SW radiation accelerating photochemical reactions of O_3 formation.

In general, increasing urban albedo is an effective strategy to mitigate UHI effect, but it worsens urban air quality. The $PM_{2.5}$ concentrations during summer and winter and the daily maximum O_3 concentrations in summer are all increased when the urban albedo increases. It is necessary to strike a balance between UHI mitigation and air quality improvement for Beijing.

5. Conclusion

We investigate the influence of land use change due to urbanization on boundary layer meteorology and air quality in Beijing using an online coupled meteorology and aerosol/chemistry model WRF-Chem. The impacts of UHI mitigation strategy (i.e., increasing urban albedo) on urban air quality are also analyzed. We pay special attention to these effects under different weather conditions (i.e., HWs in summer and polluted days in winter). Model evaluation against the observation data indicates that the WRF-Chem model captures the spatial-temporal evolutions of both meteorological and chemical parameters in Beijing fairly well.

The modification of rural land use into urban impervious surface leads to significant changes in boundary layer meteorology (temperature, relative humidity, wind speed, and PBLH) and air quality (surface-layer O_3 and $PM_{2.5}$ concentrations) in urban Beijing. The near-surface air temperature is increased by 1.8 °C in summer and 1.2 °C in winter, but a decrease is found at the higher altitudes (400–1,000 m). The changes in relative humidity are contrary to those in temperature, with a decrease of 9.5% in summer and 5.4% in winter at the height of 2 m and an increase above the height of 500 m. The increase in surface roughness in urbanized areas contributes to the decrease in WS_{10} of 0.4 m s^{-1} in summer and 0.1 m s^{-1} in winter. Enhanced turbulent mixing induced by urban sprawl leads to the increase in PLBH of 107.4 m in summer and 69.1 m in winter. The patterns of changes in surface O_3 concentrations are similar to those in temperature, with an increase of 9.5 ppbv in summer and 1.8 ppbv in winter. The surface-layer $PM_{2.5}$ concentration is decreased by 16.6 $\mu g\ m^{-3}$ in summer and 26.2 $\mu g\ m^{-3}$ in winter, which is mainly attributed to the increase in PBLH.

We also focus on these effects under different weather conditions (i.e., HWs in summer and polluted days in winter). Compared with normal days (clean days), the UHI intensity, quantified by the difference in urban-rural temperature, is enhanced by 11.1% during HWs in summer (by 16.7% during polluted days in winter). The decreases in relative humidity induced by urbanization are smaller in hot days and polluted days. The increases in PBLH due to urbanization are larger during HWs in summer but smaller during polluted days in winter. Urbanization can increase the surface-layer O_3 concentrations over the urbanized areas both in summer and winter, but the impacts are reduced during HWs and polluted days. The decreases in surface-layer $PM_{2.5}$ concentrations induced by urbanization are larger in hot days and polluted days.

Increasing urban albedo is an effective mitigation strategy to reduce UHI intensity. When the urban albedo is increased from 0.2 to 0.85, the UHI intensity is decreased by 28.0% in normal days and by 29.9% in hot days during summer, and by 64.7% in clean days and by 38.3% in polluted days during winter. Although increasing urban albedo is an effective way to decrease UHI intensity, it worsens the urban air quality. When the urban albedo is increased from 0.2 to 0.85, the daily average $PM_{2.5}$ concentrations are increased by 10.2 $\mu g\ m^{-3}$ in summer and 6.1 $\mu g\ m^{-3}$ in winter, the daily maximum O_3 concentrations are increased by 12.8 ppbv under HWs in summer.

The findings from the study have important implications for urban planning in Beijing. The adverse effects of urbanization on regional climate and air quality (and ulteriorly on human comfortableness) should not be overlooked; it is also necessary to strike a balance between UHI mitigation and air quality improvement for Beijing.

6. Discussion

There are some uncertainties in our simulation that need to be addressed in future studies:

1. The urban canopy parameters (UCPs), such as building height, street width, and surface albedo, are crucial factors and can affect the accuracy of simulation results (Chen et al., 2011; Ching, 2013). At present, the UCPs used in this study are default values taken from the WRF-Chem look-up table. More realistic and detailed gridded UCPs data should be used in future studies.
2. Model simulations with analysis nudging are preferable to those without because analysis nudging can improve initial and boundary conditions by combining high resolution upper level and surface observations with global analysis fields to generate more accurate meteorological data for air quality simulations (Lo et al., 2008; Wang, Bruyère, et al., 2009; Yegorova et al., 2011). However, Rogers et al. (2013) indicated that different nudging strategies (no FDDA, FDDA excluded from PBL, and so on) can lead to significant differences in simulation results. As compared in Table S4, simulated meteorological fields (T_2, RH_2, WS_{10}, and WD_{10}) and pollutant concentrations (O_3 and $PM_{2.5}$) in CTL (nudging at all model levels and all domains) are different from those simulated by NUDGING (nudging above the boundary layer and in outer domains; detail FDDA parameters used in the NUDGING case can be found in Table S2) at both the near surface layer and at the near PBL layer. Bowden et al. (2012) pointed out that analysis nudging applied to the inner domain can achieve a reduction of bias in basic meteorological fields compared to restricting the influence of input fields only to the outer domain, which is also supported by Table S3. However, Rogers et al. (2013) showed that the nudging method used within the atmospheric boundary layer and the inner domain may smooth the differences between control and sensitivity simulations.
3. As Akbari et al. (2016) classified that a clean, smooth, and solar-opaque white surface with a solar reflectance of nearly 0.85 can strongly reflect visible and near-infrared radiation. But this cool type is an ideal highly reflective white paint (Fallmann et al., 2016), and in reality, the albedo should be less than 0.85 mainly limited by reflective materials in addition to glare problems and aesthetic preferences (Vahmani et al., 2016). Therefore, advancements in material technology for reflective roof to mitigate the UHI have been a continued effort among scientific researchers and urban planners (Ferrari et al., 2013; Gartland, 2008; Karlessi et al., 2011; Roman et al., 2016; Santamouris et al., 2011). In addition, urban greening, another useful and practical method to mitigate the UHI intensity (Fallmann et al., 2016; Li et al., 2014), is also helpful for the improvements in urban environment (Li et al., 2010; Yang et al., 2008) because green vegetation can sequester carbon, reduce soil erosion, improve water quality, and provide habitat for wildlife and recreation for urban dwellers (Gorsevski et al., 1998). The decreased urban air temperature caused by cool roof and urban greening can further reduce the demand of cooling energy from air conditioning

in summer (Shahmohamadi et al., 2010), which also means that the emissions of air pollutants from electricity generation by power plants may become lower (Gorsevski et al., 1998). However, the decreased air temperature can also affect the atmospheric boundary layer, including reduced vertical mixing, lower boundary layer depth, and weaker convective rolls. The lowered horizontal wind speeds and vertical mixing make the atmosphere near the surface to be stagnant, which may potentially cause air quality issues (Sharma et al., 2016). These competing feedbacks will be considered in our future study in detail.

4. With the acceleration of industrialization and urbanization in China, anthropogenic and biogenic emissions have changed a lot. Jiang et al. (2017) concluded that the increase of urban land cover leads large surface warming, while anthropogenic aerosols cause widespread cooling at the surface. Their joint effect on the surface temperature and the circulation is dominated by the aerosols' effect with a reduced magnitude. Chen et al. (2014) reflected that, although the impacts of land use changes on air quality are non-negligible, the emission distribution and emission load exert a more significant influence on air quality than the land use change. Therefore, a further discussion about the urbanization impacts associated with the changes of anthropogenic and biogenic emissions on boundary layer meteorology and air quality will be studied in our future work.
5. Facing the Bohai Sea, Beijing is frequently influenced by the sea-land breeze circulations. What is more, Beijing is surrounded by mountains on three sides, and therefore, it is also affected by the mountain-valley breeze circulations. The rapid urbanization process of Beijing leads to the formation of UHI circulations. Quantifying the combined effects of the three circulations on regional climate and air quality over Beijing will be an interesting research topic.

Acknowledgments

This work was supported by the Strategic Priority Research Program of the Chinese Academy of Sciences (XDA19040204), the National Natural Science Foundation of China (91544221 and 41675016), and the Russian Science Foundation under grant 14-47-00049. The daily meteorological observations can be collected from http://www.wunderground.com (for ground-level data) and http://weather.uwyo.edu/upperair/sounding.html (for sounding data). The China National Environmental Monitoring Center (CNEMC, http://113.108.142.147:20035/emcpublish/) provides the hourly O_3 and $PM_{2.5}$ concentrations. The AERONET Level 2.0 AOD data are downloaded from https://aeronet.gsfc.nasa.gov/. Hourly downward solar radiation flux at the Xianghe station is taken from World Radiation Monitoring Center-Baseline Surface Radiation Network (WRMC-BSRN, http://bsrn.awi.de), or readers can contact the contributor Xiang'ao Xia (xxa@mail.iap.ac.cn, Institute of Atmospheric Physics, Chinese Academy of Sciences) to obtain the data. Data used to generate figures and tables from the WRF-Chem model in this manuscript are available freely upon request from the authors via mgzhang@mail.iap.ac.cn and chenlei@mail.iap.ac.cn or can be downloaded at https://pan.baidu.com/s/4c4i1r1m. We are also very grateful to the reviewers for their helpful comments and thoughtful suggestions.

References

Akbari, H., Cartalis, C., Kolokotsa, D., Muscio, A., Pisello, A. L., Rossi, F., et al. (2016). Local climate change and urban heat island mitigation technique—The state of the art. *Journal of Civil Engineering and Management*, *22*(1), 1–16. https://doi.org/10.3846/13923730.2015.1111934

Bowden, J. H., Otte, T. L., Nolte, C. G., & Otte, M. J. (2012). Examining interior grid nudging techniques using two-way nesting in the WRF model for regional climate modeling. *Journal of Climate*, *25*(8), 2805–2823. https://doi.org/10.1175/jcli-d-11-00167.1

Cai, W., Li, K., Liao, H., Wang, H., & Wu, L. (2017). Weather conditions conducive to Beijing severe haze more frequent under climate change. *Nature Climate Change*, *7*(4), 257–262. https://doi.org/10.1038/nclimate3249

Cao, C., Lee, X., Liu, S., Schultz, N., Xiao, W., Zhang, M., & Zhao, L. (2016). Urban heat islands in China enhanced by haze pollution. *Nature Communications*, *7*, 12509. https://doi.org/10.1038/ncomms12509

Chen, B., Yang, S., Xu, X.-D., & Zhang, W. (2014). The impacts of urbanization on air quality over the Pearl River Delta in winter: Roles of urban land use and emission distribution. *Theoretical and Applied Climatology*, *117*(1–2), 29–39. https://doi.org/10.1007/s00704-013-0982-1

Chen, F., Kusaka, H., Bornstein, R., Ching, J., Grimmond, C. S. B., Grossman-Clarke, S., et al. (2011). The integrated WRF/urban modelling system: Development, evaluation, and applications to urban environmental problems. *International Journal of Climatology*, *31*(2), 273–288. https://doi.org/10.1002/joc.2158

Chen, F., Mitchell, K., Schaake, J., Xue, Y., Pan, H. L., Koren, V., et al. (1996). Modeling of land surface evaporation by four schemes and comparison with FIFE observations. *Journal of Geophysical Research*, *101*(D3), 7251–7268. https://doi.org/10.1029/95JD02165

Chen, L., Zhang, M., & Wang, Y. (2016). Model analysis of urbanization impacts on boundary layer meteorology under hot weather conditions: A case study of Nanjing, China. *Theoretical and Applied Climatology*, *125*(3-4), 713–728. https://doi.org/10.1007/s00704-015-1535-6

Chen, L., Zhang, M., Zhu, J., & Skorokhod, A. (2017). Model analysis of soil dust impacts on the boundary layer meteorology and air quality over East Asia in April 2015. *Atmospheric Research*, *187*, 42–56. https://doi.org/10.1016/j.atmosres.2016.12.008

Chen, W., Zhang, Y., Pengwang, C., & Gao, W. (2017). Evaluation of urbanization dynamics and its impacts on surface heat islands: A case study of Beijing, China. *Remote Sensing*, *9*(5), 453. https://doi.org/10.3390/rs9050453

Ching, J. K. S. (2013). A perspective on urban canopy layer modeling for weather, climate and air quality applications. *Urban Climate*, *3*, 13–39. https://doi.org/10.1016/j.uclim.2013.02.001

Chrysanthou, A., van der Schrier, G., van den Besselaar, E. J. M., Klein Tank, A. M. G., & Brandsma, T. (2014). The effects of urbanization on the rise of the European temperature since 1960. *Geophysical Research Letters*, *41*, 7716–7722. https://doi.org/10.1002/2014GL061154

Coumou, D., Robinson, A., & Rahmstorf, S. (2013). Global increase in record-breaking monthly-mean temperatures. *Climatic Change*, *118*(3-4), 771–782. https://doi.org/10.1007/s10584-012-0668-1

Ding, Y., & Liu, Y. (2014). Analysis of long-term variations of fog and haze in China in recent 50 years and their relations with atmospheric humidity. *Science China Earth Sciences*, *57*(1), 36–46. https://doi.org/10.1007/s11430-013-4792-1

Emmons, L. K., Walters, S., Hess, P. G., Lamarque, J. F., Pfister, G. G., Fillmore, D., et al. (2010). Description and evaluation of the model for ozone and related chemical tracers, version 4 (MOZART-4). *Geoscientific Model Development*, *3*(1), 43–67. https://doi.org/10.5194/gmd-3-43-2010

Fallmann, J., Forkel, R., & Emeis, S. (2016). Secondary effects of urban heat island mitigation measures on air quality. *Atmospheric Environment*, *125*, 199–211. https://doi.org/10.1016/j.atmosenv.2015.10.094

Ferrari, C., Libbra, A., Muscio, A., & Siligardi, C. (2013). Design of ceramic tiles with high solar reflectance through the development of a functional engobe. *Ceramics International*, *39*(8), 9583–9590. https://doi.org/10.1016/j.ceramint.2013.05.077

Flanner, M. G. (2009). Integrating anthropogenic heat flux with global climate models. *Geophysical Research Letters*, *36*, L02801. https://doi.org/10.1029/2008GL036465

Gaffin, S. R., Rosenzweig, C., Khanbilvardi, R., Parshall, L., Mahani, S., Glickman, H., et al. (2008). Variations in New York city's urban heat island strength over time and space. *Theoretical and Applied Climatology*, *94*(1-2), 1–11. https://doi.org/10.1007/s00704-007-0368-3

Gao, M., Carmichael, G. R., Wang, Y., Saide, P. E., Yu, M., Xin, J., et al. (2016). Modeling study of the 2010 regional haze event in the North China Plain. *Atmospheric Chemistry and Physics*, *16*(3), 1673–1691. https://doi.org/10.5194/acp-16-1673-2016

Gao, Y., Zhang, M., Liu, Z., Wang, L., Wang, P., Xia, X., et al. (2015). Modeling the feedback between aerosol and meteorological variables in the atmospheric boundary layer during a severe fog-haze event over the North China Plain. *Atmospheric Chemistry and Physics*, *15*, 4279–4295. https://doi.org/10.5194/acp-15-4279-2015

Gartland, L. (2008). *Heat islands: Understanding and mitigating heat in urban areas* (p. 58). UK: Earthscan.

Gong, S. L., Barrie, L. A., & Blanchet, J. P. (1997). Modeling sea-salt aerosols in the atmosphere: 1. Model development. *Journal of Geophysical Research*, *102*(D3), 3805–3818. https://doi.org/10.1029/96JD02953

Gorsevski, V., Taha, H., Quattrochi, D., & Luvall, J. (1998). Air pollution prevention through urban heat island mitigation: An update on the Urban Heat Island Pilot Project. *Proceedings of the ACEEE Summer Study* (Vol. 9, pp. 23–32). Asilomar, CA.

Grell, G. A., Peckham, S. E., Schmitz, R., McKeen, S. A., Frost, G., Skamarock, W. C., & Eder, B. (2005). Fully coupled "online" chemistry within the WRF model. *Atmospheric Environment*, *39*(37), 6957–6975. https://doi.org/10.1016/j.atmosenv.2005.04.027

Guenther, A., Karl, T., Harley, P., Wiedinmyer, C., Palmer, P. I., & Geron, C. (2006). Estimates of global terrestrial isoprene emissions using MEGAN (Model of Emissions of Gases and Aerosols from Nature). *Atmospheric Chemistry and Physics*, *6*(11), 3181–3210. https://doi.org/10.5194/acp-6-3181-2006

Han, X., Zhang, M., Gao, J., Wang, S., & Chai, F. (2014). Modeling analysis of the seasonal characteristics of haze formation in Beijing. *Atmospheric Chemistry and Physics*, *14*(18), 10,231–10,248. https://doi.org/10.5194/acp-14-10231-2014

Hansen, J., Ruedy, R., Sato, M., & Lo, K. (2010). Global surface temperature change. *Reviews of Geophysics*, *48*, RG4004. https://doi.org/10.1029/2010RG000345

Holben, B. N., Eck, T., Slutsker, I., Tanre, D., Buis, J., Setzer, A., et al. (1998). AERONET—A federated instrument network and data archive for aerosol characterization. *Remote Sensing of Environment*, *66*(1), 1–16. https://doi.org/10.1016/S0034-4257(98)00031-5

Holst, C. C., Tam, C.-Y., & Chan, J. C. L. (2016). Sensitivity of urban rainfall to anthropogenic heat flux: A numerical experiment. *Geophysical Research Letters*, *43*, 2240–2248. https://doi.org/10.1002/2015gl067628

Hu, Z., Zhao, C., Huang, J., Leung, L. R., Qian, Y., Yu, H., et al. (2016). Trans-Pacific transport and evolution of aerosols: Evaluation of quasi-global WRF-Chem simulation with multiple observations. *Geoscientific Model Development*, *9*(5), 1725–1746. https://doi.org/10.5194/gmd-9-1725-2016

Jacobson, M. Z., Nghiem, S. V., Sorichetta, A., & Whitney, N. (2015). Ring of impact from the mega-urbanization of Beijing between 2000 and 2009. *Journal of Geophysical Research: Atmospheres*, *120*, 5740–5756. https://doi.org/10.1002/2014jd023008

Jiang, Z., Huo, F., Ma, H., Song, J., & Dai, A. (2017). Impact of Chinese urbanization and aerosol emissions on the East Asian Summer Monsoon. *Journal of Climate*, *30*(3), 1019–1039. https://doi.org/10.1175/jcli-d-15-0593.1

Jones, P. D., Lister, D. H., & Li, Q. (2008). Urbanization effects in large-scale temperature records, with an emphasis on China. *Journal of Geophysical Research*, *113*, D16122. https://doi.org/10.1029/2008JD009916

Karlessi, T., Santamouris, M., Synnefa, A., Assimakopoulos, D., Didaskalopoulos, P., & Apostolakis, K. (2011). Development and testing of PCM doped cool colored coatings to mitigate urban heat island and cool buildings. *Building and Environment*, *46*(3), 570–576. https://doi.org/10.1016/j.buildenv.2010.09.003

Kusaka, H., & Kimura, F. (2004). Coupling a single-layer urban canopy model with a simple atmospheric model: Impact on urban heat island simulation for an idealized case. *Journal of the Meteorological Society of Japan*, *82*(1), 67–80. https://doi.org/10.2151/jmsj.82.67

Kusaka, H., Kondo, H., Kikegawa, Y., & Kimura, F. (2001). A simple single-layer urban canopy model for atmospheric models: Comparison with multi-layer and slab models. *Boundary-Layer Meteorology*, *101*(3), 329–358. https://doi.org/10.1023/A:1019207923078

Lazzarini, M., Marpu, P. R., & Ghedira, H. (2013). Temperature-land cover interactions: The inversion of urban heat island phenomenon in desert city areas. *Remote Sensing of Environment*, *130*, 136–152. https://doi.org/10.1016/j.rse.2012.11.007

Li, D., & Bou-Zeid, E. (2013). Synergistic interactions between urban heat islands and heat waves: The impact in cities is larger than the sum of its parts. *Journal of Applied Meteorology and Climatology*, *52*(9), 2051–2064. https://doi.org/10.1175/jamc-d-13-02.1

Li, D., Bou-Zeid, E., & Oppenheimer, M. (2014). The effectiveness of cool and green roofs as urban heat island mitigation strategies. *Environmental Research Letters*, *9*(5), 055002. https://doi.org/10.1088/1748-9326/9/5/055002

Li, D., Sun, T., Liu, M., Yang, L., Wang, L., & Gao, Z. (2015). Contrasting responses of urban and rural surface energy budgets to heat waves explain synergies between urban heat islands and heat waves. *Environmental Research Letters*, *10*(5), 054009. https://doi.org/10.1088/1748-9326/10/5/054009

Li, J. F., Wai, O. W. H., Li, Y. S., Zhan, J. M., Ho, Y. A., Li, J., & Lam, E. (2010). Effect of green roof on ambient CO_2 concentration. *Building and Environment*, *45*(12), 2644–2651. https://doi.org/10.1016/j.buildenv.2010.05.025

Li, M., Song, Y., Mao, Z., Liu, M., & Huang, X. (2016). Impacts of thermal circulations induced by urbanization on ozone formation in the Pearl River Delta region, China. *Atmospheric Environment*, *127*, 382–392. https://doi.org/10.1016/j.atmosenv.2015.10.075

Li, Y., Zhu, L., Zhao, X., Li, S., & Yan, Y. (2013). Urbanization impact on temperature change in China with emphasis on land cover change and human activity. *Journal of Climate*, *26*(22), 8765–8780. https://doi.org/10.1175/jcli-d-12-00698.1

Liao, J., Wang, T., Jiang, Z., Zhuang, B., Xie, M., Yin, C., et al. (2015). WRF/Chem modeling of the impacts of urban expansion on regional climate and air pollutants in Yangtze River Delta, China. *Atmospheric Environment*, *106*, 204–214. https://doi.org/10.1016/j.atmosenv.2015.01.059

Lin, C. Y., Chen, F., Huang, J. C., Chen, W. C., Liou, Y. A., Chen, W. N., & Liu, S. C. (2008). Urban heat island effect and its impact on boundary layer development and land-sea circulation over northern Taiwan. *Atmospheric Environment*, *42*(22), 5635–5649. https://doi.org/10.1016/j.atmosenv.2008.03.015

Lin, C. Y., Su, S. J., Kusaka, H., Akimoto, Y., Sheng, Y. F., Huang, J. C., & Hsu, H. H. (2016). Impact of an improved WRF urban canopy model on diurnal air temperature simulation over northern Taiwan. *Atmospheric Chemistry and Physics*, *16*(3), 1809–1822. https://doi.org/10.5194/acp-16-1809-2016

Lin, X., & Yu, S. (2005). Interdecadal changes of temperature in the Beijing region and its heat island effect. *Journal of Geophysics*, *48*(1), 47–54. https://doi.org/10.1002/cjg2.624

Lo, J. C. F., Yang, Z. L., & Pielke, R. A. (2008). Assessment of three dynamical climate downscaling methods using the Weather Research and Forecasting (WRF) model. *Journal of Geophysical Research*, *113*, D09112. https://doi.org/10.1029/2007JD009216

Mackey, C. W., Lee, X., & Smith, R. B. (2012). Remotely sensing the cooling effects of city scale efforts to reduce urban heat island. *Building and Environment*, *49*, 348–358. https://doi.org/10.1016/j.buildenv.2011.08.004

Miao, S., Chen, F., LeMone, M. A., Tewari, M., Li, Q., & Wang, Y. (2009). An observational and modeling study of characteristics of urban heat island and boundary layer structures in Beijing. *Journal of Applied Meteorology and Climatology*, *48*(3), 484–501. https://doi.org/10.1175/2008jamc1909.1

Miao, S., Chen, F., Li, Q., & Fan, S. (2011). Impacts of urban processes and urbanization on summer precipitation: A case study of heavy rainfall in Beijing on 1 August 2006. *Journal of Applied Meteorology and Climatology*, *50*(4), 806–825. https://doi.org/10.1175/2010jamc2513.1

Mölders, N., Tran, H. N. Q., Cahill, C. F., Leelasakultum, K., & Tran, T. T. (2012). Assessment of WRF/Chem PM2.5 forecasts using mobile and fixed location data from the Fairbanks, Alaska winter 2008/09 field campaign. *Atmospheric Pollution Research*, *3*(2), 180–191. https://doi.org/10.5094/apr.2012.018

National Bureau of Statistics of China (2016). *China statistical yearbook*. Beijing: China Statistics Press.

Oke, T. R. (1973). City size and the urban heat island. *Atmospheric Environment (1967)*, *7*(8), 769–779. https://doi.org/10.1016/0004-6981(73)90140-6

Otte, T. L. (2008). The impact of nudging in the meteorological model for retrospective air quality simulations. Part I: Evaluation against national observation networks. *Journal of Applied Meteorology and Climatology*, *47*(7), 1853–1867. https://doi.org/10.1175/2007jamc1790.1

Owen, T. W., Carlson, T. N., & Gillies, R. R. (1998). An assessment of satellite remotely-sensed land cover parameters in quantitatively describing the climatic effect of urbanization. *International Journal of Remote Sensing*, *19*(9), 1663–1681. https://doi.org/10.1080/014311698215171

Qian, Y., Yan, H., Berg, L. K., Hagos, S., Feng, Z., Yang, B., & Huang, M. (2016). Assessing impacts of PBL and surface layer schemes in simulating the surface-atmosphere interactions and precipitation over the tropical ocean using observations from AMIE/DYNAMO. *Journal of Climate*, *29*(22), 8191–8210. https://doi.org/10.1175/jcli-d-16-0040.1

Randerson, J. T., Van der Werf, G. R., Giglio, L., Collatz, G. J., & Kasibhatla, P. S. (2005). Global Fire Emissions Database, Version 2 (GFEDv2.1), Retrieved from http://daac.ornl.gov/ (last access: 11 November 2013), from Oak Ridge National Laboratory Distributed Active Archive Center, Oak Ridge, TN. https://doi.org/10.3334/ORNLDAAC/849

Ren, G., Zhou, Y., Chu, Z., Zhou, J., Zhang, A., Guo, J., & Liu, X. (2008). Urbanization effects on observed surface air temperature trends in North China. *Journal of Climate*, *21*(6), 1333–1348. https://doi.org/10.1175/2007jcli1348.1

Ren, G. Y., Chu, Z. Y., Chen, Z. H., & Ren, Y. Y. (2007). Implications of temporal change in urban heat island intensity observed at Beijing and Wuhan stations. *Geophysical Research Letters*, *34*, L05711. https://doi.org/10.1029/2006GL027927

Reynolds, R., Liang, L., Li, X., & Dennis, J. (2017). Monitoring annual urban changes in a rapidly growing portion of Northwest Arkansas with a 20-year Landsat record. *Remote Sensing*, *9*(1), 71. https://doi.org/10.3390/rs9010071

Rogers, R. E., Deng, A., Stauffer, D. R., Gaudet, B. J., Jia, Y., Soong, S. T., & Tanrikulu, S. (2013). Application of the Weather Research and Forecasting model for air quality modeling in the San Francisco Bay area. *Journal of Applied Meteorology and Climatology*, *52*(9), 1953–1973. https://doi.org/10.1175/JAMC-D-12-0280.1

Roman, K. K., O'Brien, T., Alvey, J. B., & Woo, O. (2016). Simulating the effects of cool roof and PCM (phase change materials) based roof to mitigate UHI (urban heat island) in prominent U.S. cities. *Energy*, *96*, 103–117. https://doi.org/10.1016/j.energy.2015.11.082

Rotach, M. W., Vogt, R., Bernhofer, C., Batchvarova, E., Christen, A., Clappier, A., et al. (2005). BUBBLE—An Urban Boundary Layer Meteorology Project. *Theoretical and Applied Climatology*, *81*(3-4), 231–261. https://doi.org/10.1007/s00704-004-0117-9

Ryu, Y. H., Baik, J. J., Kwak, K. H., Kim, S., & Moon, N. (2013). Impacts of urban land-surface forcing on ozone air quality in the Seoul metropolitan area. *Atmospheric Chemistry and Physics*, *13*(4), 2177–2194. https://doi.org/10.5194/acp-13-2177-2013

Santamouris, M., Synnefa, A., & Karlessi, T. (2011). Using advanced cool materials in the urban built environment to mitigate heat islands and improve thermal comfort conditions. *Solar Energy*, *85*(12), 3085–3102. https://doi.org/10.1016/j.solener.2010.12.023

Shahmohamadi, P., Che-Ani, A. I., Ramly, A., Maulud, K. N. A., & Mohd-Nor, M. F. I. (2010). Reducing urban heat island effects: A systematic review to achieve energy consumption balance. *International Journal of Physical Sciences*, *5*(6), 626–636.

Shao, Y. (2004). Simplification of a dust emission scheme and comparison with data. *Journal of Geophysical Research*, *109*, D10202. https://doi.org/10.1029/2003JD004372

Sharma, A., Conry, P., Fernando, H. J. S., Hamlet, A. F., Hellmann, J. J., & Chen, F. (2016). Green and cool roofs to mitigate urban heat island effects in the Chicago metropolitan area: Evaluation with a regional climate model. *Environmental Research Letters*, *11*(6), 064004. https://doi.org/10.1088/1748-9326/11/6/064004

Sharma, R., & Joshi, P. K. (2016). Mapping environmental impacts of rapid urbanization in the National Capital Region of India using remote sensing inputs. *Urban Climate*, *15*, 70–82. https://doi.org/10.1016/j.uclim.2016.01.004

Shen, H., Huang, L., Zhang, L., Wu, P., & Zeng, C. (2016). Long-term and fine-scale satellite monitoring of the urban heat island effect by the fusion of multi-temporal and multi-sensor remote sensed data: A 26-year case study of the city of Wuhan in China. *Remote Sensing of Environment*, *172*, 109–125. https://doi.org/10.1016/j.rse.2015.11.005

Skamarock, W. C., Klemp, J. B., Dudhia, J., Gill, D. O., Barker, D. M., Wang, W., & Powers, J. G. (2008). A description of the Advanced Research WRF version 2, NCAR Tech. Note, NCAR/TN-468+STR, Natl. Cent. for Atmos. Res., Boulder, CO. Retrieved from http://wrf-model.org/wrfadmin/publications.php

Smith, T. T., Zaitchik, B. F., & Gohlke, J. M. (2013). Heat waves in the United States: Definitions, patterns and trends. *Climatic Change*, *118*(3-4), 811–825. https://doi.org/10.1007/s10584-012-0659-2

Song, X., Zhang, J., AghaKouchak, A., Roy, S. S., Xuan, Y., Wang, G., et al. (2014). Rapid urbanization and changes in spatiotemporal characteristics of precipitation in Beijing metropolitan area. *Journal of Geophysical Research: Atmospheres*, *119*, 11,250–11,271. https://doi.org/10.1002/2014JD022084

Taha, H. (2008). Meso-urban meteorological and photochemical modeling of heat island mitigation. *Atmospheric Environment*, *42*(38), 8795–8809. https://doi.org/10.1016/j.atmosenv.2008.06.036

Tan, J., Zheng, Y., Song, G., Kalkstein, L. S., Kalkstein, A. J., & Tang, X. (2007). Heat wave impacts on mortality in Shanghai, 1998 and 2003. *International Journal of Biometeorology*, *51*(3), 193–200. https://doi.org/10.1007/s00484-006-0058-3

Tao, W., Liu, J., Ban-Weiss, G. A., Hauglustaine, D. A., Zhang, L., Zhang, Q., et al. (2015). Effects of urban land expansion on the regional meteorology and air quality of eastern China. *Atmospheric Chemistry and Physics*, *15*(15), 8597–8614. https://doi.org/10.5194/acp-15-8597-2015

Touchaei, A. G., Akbari, H., & Tessum, C. W. (2016). Effect of increasing urban albedo on meteorology and air quality of Montreal (Canada)—Episodic simulation of heat wave in 2005. *Atmospheric Environment*, *132*, 188–206. https://doi.org/10.1016/j.atmosenv.2016.02.033

Trewin, B. (2010). Exposure, instrumentation, and observing practice effects on land temperature measurements. *Wiley Interdisciplinary Reviews: Climate Change*, *1*(4), 490–506. https://doi.org/10.1002/wcc.46

Vahmani, P., Sun, F., Hall, A., & Ban-Weiss, G. (2016). Investigating the climate impacts of urbanization and the potential for cool roofs to counter future climate change in Southern California. *Environmental Research Letters*, *11*(12). https://doi.org/10.1088/1748-9326/11/12/124027

Wang, H. J., Chen, H. P., & Liu, J. P. (2015). Arctic sea ice decline intensified haze pollution in Eastern China. *Atmospheric and Oceanic Science Letters*, *8*, 1–9. https://doi.org/10.3878/AOSL20140081

Wang, J., Feng, J., Yan, Z., Hu, Y., & Jia, G. (2012). Nested high-resolution modeling of the impact of urbanization on regional climate in three vast urban agglomerations in China. *Journal of Geophysical Research*, *117*, D21103. https://doi.org/10.1029/2012JD018226

Wang, M., Yan, X., Liu, J., & Zhang, X. (2013). The contribution of urbanization to recent extreme heat events and a potential mitigation strategy in the Beijing-Tianjin-Hebei metropolitan area. *Theoretical and Applied Climatology*, *114*(3-4), 407–416. https://doi.org/10.1007/s00704-013-0852-x

Wang, W., Bruyère, C., Duda, M., Dudhia, J., Gill, D., Lin, H.-C., et al. (2009). Weather Research and Forecasting ARW user's manual (NCAR) 310 pp.

Wang, X., Liao, J., Zhang, J., Shen, C., Chen, W., Xia, B., & Wang, T. (2014). A numeric study of regional climate change induced by urban expansion in the Pearl River Delta, China. *Journal of Applied Meteorology and Climatology*, *53*(2), 346–362. https://doi.org/10.1175/jamc-d-13-054.1

Wang, X., Wu, Z., & Liang, G. (2009). WRF/CHEM modeling of impacts of weather conditions modified by urban expansion on secondary organic aerosol formation over Pearl River Delta. *Particuology*, *7*(5), 384–391. https://doi.org/10.1016/j.partic.2009.04.007

Wang, X. M., Lin, W. S., Yang, L. M., Deng, R. R., & Lin, H. (2007). A numerical study of influences of urban land-use change on ozone distribution over the Pearl River Delta region, China. *Tellus Series B: Chemical and Physical Meteorology*, *59*(3), 633–641. https://doi.org/10.1111/j.1600-0889.2007.00271.x

Wu, L., Su, H., Jiang, J. H., & Read, W. G. (2012). Hydration or dehydration: Competing effects of upper tropospheric cloud radiation on the TTL water vapor. *Atmospheric Chemistry and Physics*, *12*(16), 7727–7735. https://doi.org/10.5194/acp-12-7727-2012

Xie, Y., Sha, Z., & Yu, M. (2008). Remote sensing imagery in vegetation mapping: Areview. *Journal of Plant Ecology*, *1*(1), 9–23. https://doi.org/10.1093/jpe/rtm005

Yan, Z., Li, Z., Li, Q., & Jones, P. (2009). Effects of site change and urbanization in the Beijing temperature series 1977–2006. *International Journal of Climatology*, *30*(8), 1226–1234. https://doi.org/10.1002/joc.1971

Yang, J., Yu, Q., & Gong, P. (2008). Quantifying air pollution removal by green roofs in Chicago. *Atmospheric Environment*, *42*(31), 7266–7273. https://doi.org/10.1016/j.atmosenv.2008.07.003

Yang, L., Niyogi, D., Tewari, M., Aliaga, D., Chen, F., Tian, F., & Ni, G. (2016). Contrasting impacts of urban forms on the future thermal environment: Example of Beijing metropolitan area. *Environmental Research Letters*, *11*(3), 034018. https://doi.org/10.1088/1748-9326/11/3/034018

Yang, L., Smith, J. A., Baeck, M. L., Bou-Zeid, E., Jessup, S. M., Tian, F., & Hu, H. (2014). Impact of urbanization on heavy convective precipitation under strong large-scale forcing: A case study over the Milwaukee-Lake Michigan Region. *Journal of Hydrometeorology*, *15*(1), 261–278. https://doi.org/10.1175/jhm-d-13-020.1

Yang, X., Hou, Y., & Chen, B. (2011). Observed surface warming induced by urbanization in east China. *Journal of Geophysical Research*, *116*, D14113. https://doi.org/10.1029/2010JD015452

Yegorova, E. A., Allen, D. J., Loughner, C. P., Pickering, K. E., & Dickerson, R. R. (2011). Characterization of an eastern U.S. severe air pollution episode using WRF/Chem. *Journal of Geophysical Research*, *116*, D17306. https://doi.org/10.1029/2010JD015054

Zaveri, R. A., Easter, R. C., Fast, J. D., & Peters, L. K. (2008). Model for Simulating Aerosol Interactions and Chemistry (MOSAIC). *Journal of Geophysical Research*, *113*, D13204. https://doi.org/10.1029/2007JD008782

Zaveri, R. A., & Peters, L. K. (1999). A new lumped structure photochemical mechanism for large-scale applications. *Journal of Geophysical Research*, *104*(D23), 30,387–30,415. https://doi.org/10.1029/1999JD900876

Zhang, N., Gao, Z., Wang, X., & Chen, Y. (2010). Modeling the impact of urbanization on the local and regional climate in Yangtze River Delta, China. *Theoretical and Applied Climatology*, *102*(3-4), 331–342. https://doi.org/10.1007/s00704-010-0263-1

Zhang, N., Wang, X., Chen, Y., Dai, W., & Wang, X. (2015). Numerical simulations on influence of urban land cover expansion and anthropogenic heat release on urban meteorological environment in Pearl River Delta. *Theoretical and Applied Climatology*, *126*, 469–479. https://doi.org/10.1007/s00704-015-1601-0

Zhang, Y., Dubey, M. K., Olsen, S. C., Zheng, J., & Zhang, R. (2009). Comparisons of WRF/Chem simulations in Mexico City with ground-based RAMA measurements during the 2006-MILAGRO. *Atmospheric Chemistry and Physics*, *9*(11), 3777–3798. https://doi.org/10.5194/acp-9-3777-2009

Zhang, Y. Z., Miao, S. G., Dai, Y. J., & Liu, Y. H. (2013). Numerical simulation of characteristics of summer clear day boundary layer in Beijing and the impact of urban underlying surface on sea breeze. *Chinese Journal of Geophysics-Chinese Edition*, *56*(8), 2558–2573. https://doi.org/10.6038/cjg20130806

Zhou, D., Zhao, S., Liu, S., Zhang, L., & Zhu, C. (2014). Surface urban heat island in China's 32 major cities: Spatial patterns and drivers. *Remote Sensing of Environment*, *152*, 51–61. https://doi.org/10.1016/j.rse.2014.05.017

Zhu, B., Kang, H., Zhu, T., Su, J., Hou, X., & Gao, J. (2015). Impact of Shanghai urban land surface forcing on downstream city ozone chemistry. *Journal of Geophysical Research: Atmospheres*, *120*, 4340–4351. https://doi.org/10.1002/2014JD022859